CHARACTERIZATION OF A PLEIOTROPIC PROTEIN PROMOTING REPAIR

CHARACTERIZATION OF A PLEIOTROPIC PROTEIN PROMOTING DNA REPAIR

BY MATTHEW CZERWINSKI, B.SC.

A Thesis Submitted to the School of Graduate Studies
in Partial Fulfillment of the Requirements
for the Degree Master of Science

McMaster University

Master of Science (2013) McMaster University

Biochemistry and Biomedical Sciences Hamilton, Ontario, Canada

TITLE: Characterization of a Pleiotropic Protein Promoting DNA Repair

AUTHOR: Matthew Czerwinski, B.Sc. (Brock University)

SUPERVISOR: Dr. Murray S. Junop

NO. OF PAGES: xiv, 103

ABSTRACT

DNA double-strand breaks (DSBs) represent the most severe form of chromosomal damage. In higher organisms, one DSB represents a lethal event. Unlike any other organism, bacteria of the genus *Deinococcus* are able to withstand extremely high levels of DSBs caused by ionizing radiation, UV radiation, prolonged desiccation and chemical agents. The remarkable ability of *Deinococcus* to survive under conditions of extreme oxidative stress is a result of an efficient DSB repair process. Currently, little is known about how several key proteins function in DNA repair in *Deinococcus*. The goal of this work was to better understand the mechanism through which *Deinococcus* is able to recover from DNA damage through structural and biochemical characterization of a unique pleiotropic protein promoting DNA repair. Here, we show preliminary X-ray diffraction data coupled with electron microscopy images which showcase unusual filament formation of this protein. Pleiotropic protein promoting DNA repair has been shown by others to bind double-stranded DNA (dsDNA). We have further characterized the interaction of this protein with DNA and found that it binds longer pieces of dsDNA (> 3500 bp) with a higher affinity than shorter pieces of dsDNA (≤ 1000 bp). This protein was also shown to form bundles of long, fibrous filaments by transmission electron microscopy, while gel filtration studies have shown it exists as a very large multimer in solution. Implications for how these filaments function in DNA repair were explored. *In vivo* damage recovery through complementation studies were also performed. Determining

the structure of pleiotropic protein promoting DNA repair, and characterizing its DNA binding ability and filament formation is essential to clarify its proposed function in DNA repair.

ACKNOWLEDGEMENTS

I would like to begin by thanking Dr. Murray Junop for the opportunity to pursue Graduate studies in his lab. Your passion, enthusiasm, and never-ending optimism spurred my interest and excitement in this project. I admired your open-door policy when it came to discussing science and non-science matters, and it was a privilege to call you “boss”. I would also like to thank my committee members, Drs. Lori Burrows, and Joaquin Ortega. Our discussions were always thought-provoking, and helped to guide and strengthen this thesis.

To the Graduate and Undergraduate students who came through the Junop Lab during my studies – thank you. Every one of you has affected me in one way or another. In particular, I would like to thank Dr. Seiji Sugiman-Marangos, who laid the foundation on which I have built. I am grateful for your teaching, advice and insight into my project.

I would like to thank my family: my mother, Teresa Czerwinski, and sister, Natalie Czerwinski. Your unconditional love and support were always strong, even when I got lost in my work. To Carolyn Dowling and Courtney Osborn, your constant encouragement was always appreciated. Most importantly, thank you to Michelle Dowling. Though many people questioned our decision to do this together, I never doubted it once. You were my built-in support system; the perfect lab mate - but an even better life mate, and I am very excited for our future together.

DECLARATION OF ACADEMIC ACHIEVEMENT

The majority of the work presented in this thesis was done independently by the author. Other significant contributions were made by Alexa Mordhorst, who purified PprA and carried out crystallography trials with $PprA_{9-284}$ from *Deinococcus radiodurans*. Daniel Newsted was involved in characterizing the DNA binding activity of $PprA_{9-284}$, as well as crystallographic trials with full-length PprA from *Deinococcus peraridilitoris*.

Carbon-coated grids for EM studies were prepared by Marcia Reid at the Electron Microscopy Facility in the Faculty of Health Science at McMaster University.

TABLE OF CONTENTS

LIST OF FIGURES

LIST OF TABLES

LIST OF ABBREVIATIONS

Å	angstrom
AFM	atomic force microscopy
AP site	apurinic or apyrimidinic site
BER	base excision repair
D_{10}	dose yielding 10% survival
DNA	deoxyribonucleic acid
DSB	double-strand break
dsDNA	double-stranded DNA
DTT	dithiothreitol
E. coli	*Escherichia coli*
EDTA	ethylenediaminetetraacetic acid
EM	electron microscopy
EMSA	electrophoretic mobility shift assay
ESDSA	extended synthesis dependent strand annealing
FPLC	fast performance liquid chromatography
GST	glutathione-s-transferase
Gy	Gray
h	hours
H_2O	water
H_2O_2	hydrogen peroxide
His_6	hexa-histidine
HR	homologous recombination
ICL	interstrand cross-link
IMAC	immobilized metal affinity chromatography
IPTG	isopropyl β-D-thiogalactopyranoside

IR	ionizing radiation
J/m^2	Joules per minute squared
kb	kilobase
kDa	kilo-Dalton
kGy	kilo-Gray
kV	kilo-volt
λ	wavelength
LN_2	liquid nitrogen
LB	Luria Bertani
M	molar
MBP	maltose binding protein
min	minutes
mL	milli-litre
mM	milli-molar
MMC	mitomycin C
MMR	mismatch repair
Mn	manganese
MWCO	molecular weight cut-off
NER	nucleotide excision repair
$(NH_4)_2SO_4$	ammonium sulfate
NHEJ	nonhomologous end-joining
Ni	nickel
nm	nanometre
$^1O_2$	singlet oxygen
$O_2 \bullet^-$	superoxide radical
OD	optical density
OH•	hydroxyl radical
PAGE	polyacrylamide gel electrophoresis
PCR	polymerase chain reaction
PEG	polyethylene glycol
PMSF	phenylmethanesulphonylfluoride
PprA	protein promoting repair A
psi	pounds per square inch
RecA	recombinase A
ROS	reactive oxygen species
SDS	sodium dodecyl sulfate
spp.	species
ssDNA	single-stranded DNA

TBE	tris/borate/EDTA
TEM	transmission electron microscopy
TEV	tobacco etch virus
TGY	tryptone glucose yeast
UA	uranyl acetate
μm	micro-metre
μM	micro-molar
UV	ultraviolet
V	volt
WT	wild type

CHAPTER 1 – INTRODUCTION

CHAPTER 1. INTRODUCTION

1.1 DNA DAMAGE

Deoxyribonucleic acid (DNA) is a macromolecule which stores the genetic code of life. DNA contains information required to make proteins, which control the development and function of every cell in an organism. Despite its importance, DNA is susceptible to many forms of damage caused by both internal metabolic (endogenous) and external (exogenous) sources. Incorrect repair of damaged DNA can lead to loss of important genetic information, chromosomal rearrangement, or even cell death (Pardo *et al*., 2009). Therefore, it is imperative for cells to correctly repair damaged DNA in order to sustain proper cell growth and viability.

1.2 DOUBLE-STRAND BREAKS

The most labile bond in a DNA molecule is the N-glycosidic bond, which attaches the nitrogenous base of a nucleotide to the sugar-phosphate backbone. Hydrolysis of the N-glycosidic bond can result in the removal of a nitrogenous base from the DNA strand, leaving an apurinic or apyrimidinic (AP) site when an adenine/guanine or thymine/cytosine, respectively, are cleaved. The presence of AP sites is problematic, as DNA polymerases can stall at the AP site, preventing further DNA replication. Furthermore, the chemical decomposition of AP sites produces nicks in the DNA backbone which can ultimately lead to the most severe form of DNA damage, a double-strand break (DSB).

DSBs occur when nicks or single-strand breaks are generated on complementary strands of DNA within close enough proximity that base pairing and chromatin structure are incapable of keeping DNA ends physically together. DSBs most often occur when cells are in S-phase, as DNA is more susceptible to breakage while it is unraveling for use as a template for DNA replication (Symington and Gautier, 2011). Other times, alternate secondary structures of DNA may prevent replication machinery from processing the DNA, causing replication fork collapse, resulting in a DSB (Kuzminov *et al*., 1995). Although much less frequent than other forms of damage, a DSB represents the most harmful form of DNA damage (Hutchinson *et al*., 1985). A single unrepaired DSB is lethal to unicellular organisms such as *E. coli*, while only a few DSBs are lethal in nearly all other living organisms (Krasin and Hutchinson, 1977). As such, it is critical that a cell repair DSBs in order to maintain proper cellular function.

1.3 REACTIVE OXYGEN SPECIES

AP sites are formed from the hydrolytic cleavage of N-glycoside bonds. This hydrolytic cleavage is caused by reactive oxygen species (ROS). ROS are highly reactive, oxygen-containing molecules, which are generated endogenously as by-products of regular cell metabolism. Other sources of ROS include exogenous sources, such as ionizing radiation (IR), produced by the decay of radioactive elements. The ionization of water (H_2O), for example, generates highly reactive hydroxyl radicals (OH•) (Repine *et al*., 1981) which can directly or

indirectly damage DNA. Superoxide radicals ($O_2^{\bullet -}$), hydrogen peroxide (H_2O_2), and singlet oxygen ($^1O_2$), which form from the precursors generated from the radiolysis of water, are other examples of ROS that can cause DNA damage (Imlay *et al*., 2003).

Under conditions of oxidative stress (IR exposure, UV exposure, desiccation), cells produce elevated levels of ROS, thereby increasing the amount of DNA damaging agents in the cells (Imlay *et al*., 2003). Most commonly, DNA damage by ROS occurs in the form of nucleotide base modifications, such as methylation, deamination, or oxidation. Other types of DNA damage include, but are not limited to, mispairing between bases; cross-linked nucleotides including both intra- and inter-strand covalent linkages; and single- and double-strand breaks.

1.4 DNA REPAIR

To combat the various types of DNA damage that can occur, cells employ multiple repair processes that prevent detrimental downstream effects. For each type of DNA damage, the cell has evolved a specific method of repairing the damage or eliminating the source of damage. These repair processes include mismatch repair (MMR), base excision repair (BER), and nucleotide excision repair (NER) pathways. To contend with the most serious DNA lesion, the DSB, cells use two major pathways to repair the damage; homologous recombination (HR), and nonhomologous end-joining (NHEJ). DSB repair typically proceeds

through HR when the cell is in late S or G2 phase (Symington and Gautier, 2011). HR relies on the presence of an intact homologous DNA molecule to act as a template to restore the DNA sequence at the damaged site in a precise, error-free manner (Stracker and Petrini, 2011). DSB repair occurs via the NHEJ pathway at other points of the cell cycle when sister chromatids are not available for use as HR templates (Symington and Gauter, 2011). In contrast to HR, NHEJ does not require a second homologous copy of template DNA to join two contiguous fragments. Rather, in NHEJ, two broken DNA ends undergo direct ligation to mend the lesion. The two severed ends are joined together by DNA Ligase IV, and a cascade of other DNA repair proteins and factors. Since the broken DNA ends get trimmed, and gaps are filled in, the NHEJ pathway can be error-prone, and thus, is less accurate than DSB repair via HR.

1.5 *DEINOCOCCUS*

DSBs constitute the most severe form of DNA damage. In higher eukaryotes, a single unrepaired DSB can result in cell lethality. This severity is broadly conserved with sensitivities ranging from one, to only a few DSBs. One unique family of bacteria, the *Deinococcaceae*, represent an unusual exception, possessing the remarkable ability to withstand extremely high levels; over 200 DSBs per cell (Cox and Battista, 2005).

The earliest identified, and most well-studied of the *Deinococcus* species (spp.), *D. radiodurans*, was discovered in a can of spoiled ground meat which

had been irradiated with 4 kGy of γ-radiation to achieve sterility (Anderson *et al*., 1956). *D. radiodurans* has since been used as the model organism to study the extraordinary repair capabilities of this family of bacteria.

The *Deinococcus* genus currently contains 48 species, discovered in a variety of habitats such as animal guts, hot springs, cold and hot deserts, and alpine environments (Slade and Radman, 2011). The complete genomes of six *Deinococcus* spp. have been sequenced, including *D. radiodurans* R1, isolated from canned meat (White *et al*., 1999), *D. geothermalis* DSM11300, isolated from a hot spring (Makarova *et al*., 2007), *D. deserti* VCD115, isolated from the Sahara desert (de Groot *et al*., 2009), *D. maricopensis* LB-34, isolated from the Sonoran desert (Pukall *et al*., 2011), *D. proteolyticus* MRP, isolated from the feces of *Lama glama* (Copeland *et al*., 2012), and *D. gobiensis* I-0, isolated from the cold Gobi desert (Yuan *et al*., 2012). All *Deinococcus* spp. are distinguished by their ability to withstand extreme levels of exposure to DNA damaging agents (Slade and Radman, 2011).

D. radiodurans is extremely resistant to various forms of DNA damage. IR and desiccation generate DSBs, SSBs, and base damage; mitomycin C (MMC) generates DNA interstrand cross-links (ICLs), UV radiation causes formation of pyrimidine dimers; and metabolic ROS induces severe base and nucleotide damage (Slade and Radman, 2011). Although able to withstand the effects of DNA damage caused by these sources, *Deinococcus* spp. are best characterized

for their unparalleled resistance to the effects of IR (Battista 1997; Blasius *et al*., 2008; Cox and Battista, 2005).

The γ-irradiation survival curves of exponentially growing *D. radiodurans* cells display a shoulder of resistance of 5,000 Gy, with no measurable loss of viability (Moseley *et al*., 1971). The radiation dose yielding 10% survival (D_{10}) of *D. radiodurans* is 7,000 Gy (Battista, 1997), though others have reported a D_{10} as high as 10,000 Gy (Ito *et al*., 1983). For comparison, the γ-radiation D_{10} for humans is 5 Gy, and an acute exposure to only 8 Gy of γ-radiation is lethal (Arrage *et al*, 1993).

Exposure of *Deinococcus* spp. to extreme doses of IR introduces hundreds of DSBs to the chromosomal DNA. The rate and amount of DSBs formed is proportional to the γ-radiation dose (Burrell *et al*., 1971). It is important to note that *Deinococcus* spp. do not prevent the formation of DSBs, and are observed to accumulate damage at the same rate as other, non-radiation resistant bacteria (Gerard *et al*., 2001; Cox and Battista, 2005). Resistance to extreme IR, therefore, is a result of a robust DNA repair pathway(s), rather than DNA damage prevention.

Although traditional repair mechanisms appear to be active in all *Deinococcus* spp. (Makarova *et al*., 2001), the speed and accuracy of repair displayed are inconsistent with all previously characterized pathways (Cox and Battista, 2005).

Despite being broken into hundreds of small fragments, *D. radiodurans* readily reassembles its DNA back into a fully functional genome (Zahradka *et al*., 2006). This feat has been attributed to the combination of proteome protection from oxidative stress (Daly *et al*., 2004; Daly *et al*., 2007), and an efficient DNA repair process that accomplishes error free reassembly of broken DNA fragments (Minton, 1994; Daly and Minton, 1996).

Various hypotheses have been put forth to explain the extreme IR resistance of *D. radiodurans*. These include the presence of multiple genome copies (Makarova *et al*., 2001), and the condensed nature of the *Deinococcus* genome (Levin-Zaidman *et al*., 2003).

D. radiodurans has as few as two and as many as ten genome copies at a given time, depending on its growth stage (Slade and Radman, 2010). It has been suggested that multiple genome copies play a role in the radiation resistance of *D. radiodurans,* facilitating DNA repair through HR by providing repetitive DNA sequences necessary to serve as templates for repair (Hansen *et al*., 1978). However, there was no significant difference in post-irradiation viability between cells containing two genome copies, and those containing ten. Furthermore, genome multiplicity alone is insufficient to account for IR resistance, as *E. coli*, for example, contain multiple genome copies, and are not radiation resistant.

Bacterial chromosomes arrange into structures called nucleoids. The *D. radiodurans* genome adopts a very tightly structured ring-like nucleoid, which reveals a high degree of condensation that remains unaltered after a high dose of γ-radiation (Levin-Zaidman *et al*., 2003; Zimmerman *et al*., 2005). The condensed ring-like nucleoid of *D. radiodurans* was proposed to restrict the diffusion of broken DNA fragments, and maintain the linear continuity of the genome when fragmented. By maintaining linear continuity of the genome, broken DNA ends could be kept aligned for efficient repair during HR (Zimmerman *et al*., 2005). The condensed nature of the genome has also been suggested to protect DNA fragments from free radicals generated in the cytoplasm by water radiolysis, and limits accessibility to degradation enzymes (Zimmerman *et al*., 2005; Levin-Zaidman *et al*., 2003).

These theories however, have since been disproven since *D. radiodurans* cultures grown in TGY broth contain cells without ring-like nucleoids, yet are more resistant than cultures grown in a defined minimal medium containing cells with ring-like nucleoids (Daly *et al*., 2004). Apart from only a few *Deinococcus* spp., other radiation resistant species such as *D. radiopugnans* and *D. geothermalis* lack the characteristic nucleoid organization observed in *D. radiodurans* (Zimmerman *et al*., 2005) Finally, cryoelectron microscopy of vitreous sections (CEMOVIS) revealed that DNA fragments resulting from γ-irradiation are diffusible, and are not maintained in the predicted continuous linear manner (Eltsov *et al*., 2005).

1.6 PROTECTION AGAINST OXIDATIVE DAMAGE

IR induces elevated levels of ROS in cells, which cause extensive DNA damage to cellular structures. Although radiation resistant and non-radiation resistant bacteria are equally susceptible to the accumulation of DSBs induced by IR, the amount of protein damage sustained in radiation sensitive organisms is more pronounced. This observation has established the belief that protein oxidation is the main cause of radiation-induced cell death, and the capacity to prevent and tolerate protein damage is a major determinant of radiation resistance.

To prevent ROS-mediated damage, cells protect themselves with an arsenal of antioxidant enzymes and non-enzymatic ROS scavengers (Tian *et al*., 2004). Enzymes such as catalase and superoxide dismutase (SOD) protect cells from ROS-mediated damage. SOD catalyzes the conversion of $O_2^{\bullet -}$ to H_2O_2, eliminating superoxide radicals from cells. H_2O_2 is subsequently transformed into H_2O and O_2 by either catalase or peroxidase enzymes. *D. radiodurans* has high levels of constitutive catalase and SOD activity. Despite this, catalase and SOD expression levels are induced after irradiation (Liu *et al*., 2003; Tanaka *et al*., 2004). Not surprisingly, inactivation of catalase and SOD genes in *D. radiodurans* results in increased sensitivity to IR, compared to wild type (Markillie *et al*., 1999).

D. radiodurans also encodes other oxidative defense proteins, such as glutaredoxin, thioredoxin, athioredoxin reductase, and alkyl hydroperoxide reductase, which revert oxidized species back to their reduced states (White *et al*., 1999).

Non-enzymatic antioxidant species, termed ROS scavengers, also protect proteins from radiation-induced oxidative damage (Daly *et al*., 2007). Among these, divalent manganese (Mn^{2+}) complexes stand out as the most powerful antioxidants in *D. radiodurans* (Daly *et al*., 2010).

In vitro, Mn^{2+} can scavenge $O_2\bullet^-$ in complex with phosphate (Archibald *et al*., 1982; Barnese *et al*., 2008) and H_2O_2 in complex with bicarbonate and amino acids or peptides (Berlett *et al*., 1990). In *D. radiodurans*, orthophosphate acts synergistically with Mn^{2+}, forming Mn^{2+}-orthophosphate, which scavenges $O_2\bullet^-$ species. Nucleosides in *D. radiodurans*, such as uridine, also form complexes with Mn^{2+} and orthophosphate, which scavenge ROS more efficiently than Mn^{2+}-orthophosphate alone, but less efficiently than Mn^{2+}-orthophosphate-peptide complexes (Daly *et al*., 2010).

The scavenging of $O_2\bullet^-$ *in vitro* is dependent on a threshold concentration of manganese. *D. radiodurans* has exceptionally high intracellular manganese levels (0.2 to 4 mM) and a high intracellular manganese to iron (Mn/Fe) ratio of 0.24 (Daly *et al*., 2004). A high Mn/Fe ratio correlates with extreme levels of IR and desiccation resistance among bacteria (Daly *et al.*, 2004) as well as a low

level of oxidative protein damage (Daly *et al*., 2007). *D. radiodurans* contains an intracellular concentration of Mn approximately 300 times higher, and an intracellular concentration of Fe approximately 3 times lower, than the most radiation sensitive species (Daly *et al*., 2007). Furthermore, Mn is required for post-IR recovery, as *D. radiodurans* cells incubated without Mn display a 1000-fold reduction in cell survival compared to cells recovered in Mn-containing TGY media, following a dose of 10 kGy γ-irradiation (Daly *et al.*, *2004*).

D. radiodurans are also able to cleanse cells of toxic products by eliminating macromolecules damaged by ROS. This process involves the degradation and export of damaged DNA, as well as the degradation of damaged proteins. Oxidized nucleotides are detoxified and recycled by Nudix hydrolases (Bessman *et al*., 1996; Xu *et al*., 2001) and nucleotidases (Kota *et al*., 2010), while oxidized proteins are degraded by proteases (Servant *et al*., 2007). Oxidative damage in proteins alters their catalytic activities, which can lead to the disruption of cellular functions. Since oxidatively damaged proteins are dysfunctional, they need to be proteolytically removed and rapidly re-synthesized. The level of intracellular proteolytic activity is increased following IR exposure, leading to the removal of modified, inactive, or otherwise damaged proteins. (Daly *et al*., 2007; Joshi *et al*., 2004). For both radiation resistant and non-resistant organisms, the amount of oxidatively damaged proteins increases with IR and UV dose, and is negatively correlated with survival (Krisko *et al*., 2010).

Although they efficiently protect proteins against oxidative damage, neither manganese nor any other antioxidant agent seems to protect DNA from DSBs during irradiation. The numbers of DSBs per Gy per genome are similar for radiation resistant and radiation sensitive species. Therefore, it is a combination of proteome protection from oxidative stress, cellular cleansing of damaged macromolecules, and an efficient DNA repair mechanism(s) that account for the remarkable ability to withstand massive amounts of DNA damage from IR exposure.

1.7 DNA DSB REPAIR IN *DEINCOCCUS*

DSB repair in *D. radiodurans* begins with the RecFOR pathway (Figure 1.1). Upon random genome fragmentation, duplex DNA is unwound by the helicase UvrD, initiating the RecFOR pathway (Bentchikou *et al*., 2010). The DNA is then processed by the exonuclease RecJ in a 5' to 3' direction, generating 3' ssDNA overhangs. Exposed 3' ssDNA strands are coated with either single-strand binding protein (SSB), or the *Deinococcus*-specific protein, DdrB (Norais *et al*., 2009), both of which are highly induced in response to IR. DdrB appears to have a stronger affinity for ssDNA than SSB. This feature makes it more difficult for RecA to displace DdrB from ssDNA. DdrB can readily displace RecA from ssDNA (Norais *et al*., 2009).

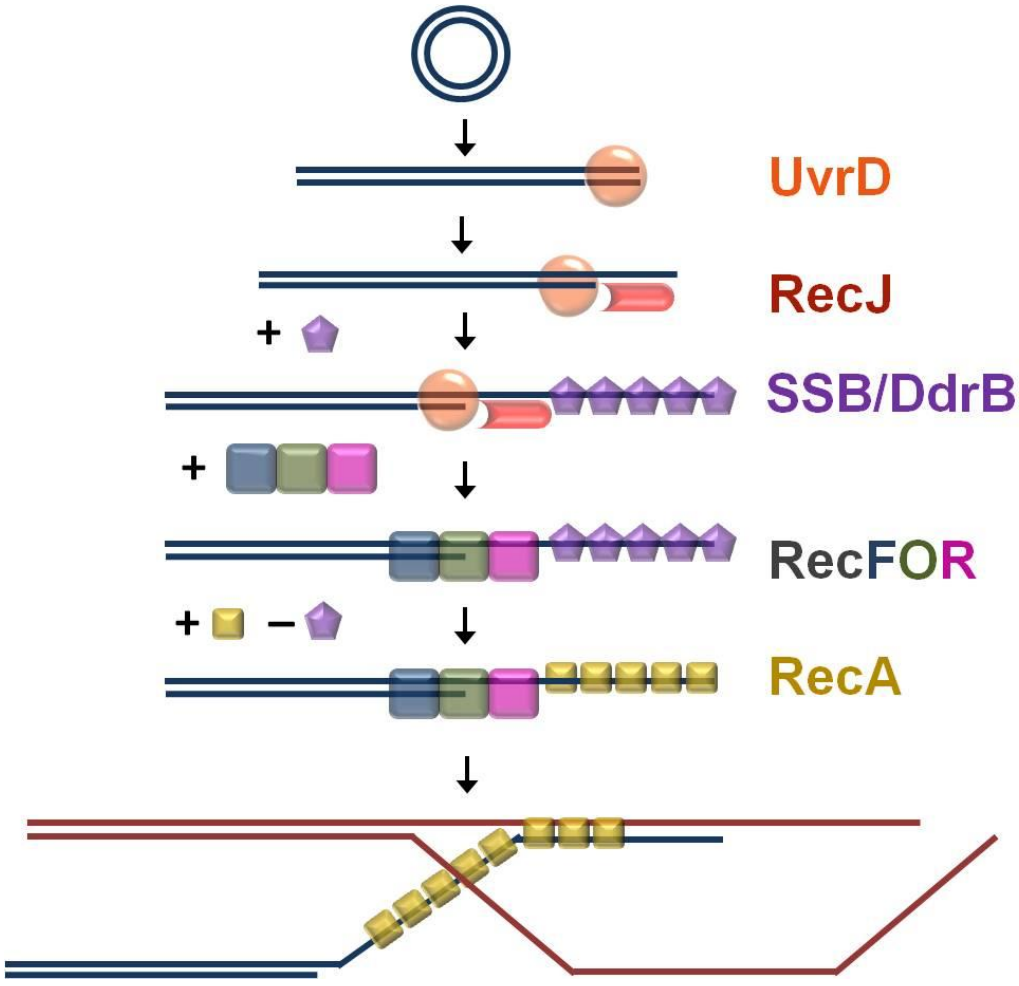

Figure 1.1 – Initiation of DSB repair in *D. radiodurans* via the RecFOR pathway. Upon fragmentation, broken DNA ends are bound by UvrD, which unwinds the duplex, while RecJ resects the DNA in a 5' to 3' direction. RecF, RecO and RecR load RecA onto ssDNA coated by SSB or DdrB, before strand exchange by homologous pairing of ssDNA and dsDNA.

The RecFOR complex loads RecA onto the 3' ssDNA coated with SSB or DdrB (Morimatsu *et al*., 2003). RecF binds to the ssDNA-dsDNA junction, and promotes the assembly of the RecOR complex, which binds onto the junction.

RecOR displaces SSB proteins and loads RecA onto 3' ssDNA (Timmins *et al*., 2007). Overall, the loading of RecA at the processed DSB site is mediated by RecR interactions with RecO, which binds SSB-coated ssDNA.

RecA forms a nucleoprotein filament that conducts a search for homology in dsDNA (Anderson and Kowalczykowski, 1997). The nucleoprotein filament aligns the bound ssDNA with a homologous duplex and promotes strand exchange. The RecA-mediated invasion of a homologous duplex by ssDNA forms a D-loop (Cox *et al*., 2000). In DNA strand exchange reactions, SSB or DdrB is required to protect ssDNA from nucleolytic degradation and remove secondary structure in the ssDNA to allow complete RecA filament formation (Kowalczykowski *et al*., 1994). SSB blocks the reversal of the strand exchange reaction by binding to the displaced strand (Lavery *et al*., 1992).

Following RecA-mediated strand invasion, DSB repair proceeds predominantly through the Extended Synthesis Dependent Strand Annealing (ESDSA) pathway. Following strand invasion, DNA synthesis is initiated by DNA Polymerase III, and can be subsequently continued by DNA Polymerase I or III. DNA Polymerase I, however, lacks the ability to initiate DNA synthesis (Slade *et al*., 2009). Extensive DNA synthesis generates long newly synthesized DNA strands, which processively dissociate from the migrating D-loops, aided by DNA helicases, and can readily anneal with complementary strands. Long linear

intermediates generated as a result of ESDSA are reassembled into circular chromosomes by RecA-dependent crossovers (Zahradka *et al*., 2006).

1.8 RecA-INDEPENDENT PATHWAY OF DSB REPAIR IN *D. RADIODURANS*

In the absence of RecA, DSBs can be repaired via a RecA-independent pathway (Daly and Minton, 1996; Minton, 1994; Slade *et al*., 2009). The mechanism of RecA-independent repair is kinetically separate from that of RecA-dependent repair, with the absence of significant DNA synthesis and a lesser extent of DNA degradation (Slade *et al*., 2009). The DSB repair pathway void of RecA, in the *recA* mutant and in the wild type at early post-IR times, consists of single-strand annealing (SSA) reactions (Daly and Minton, 1996). After resection of DNA ends, single-stranded overhangs are produced, as in the RecFOR pathway. If the overhangs contain complementary sequences, they can anneal, resulting in long dsDNA intermediates. In WT cells, early annealing reactions would increase the physical length of many chromosomal DNA fragments, thereby reducing the damage caused by exonucleases and facilitating RecA-mediated DNA repair via the ESDSA pathway.

1.9 TRANSCRIPTOME ANALYSIS OF *D. RADIODURANS*

Whole genome sequencing of *D. radiodurans* and *D. geothermalis* was conducted for comparative genome analysis, to identify genes responsible for the radiation resistance observed in *Deinococcus* spp. (White *et al*., 1999, Appukuttan *et al*., 2006). Although *D. radiodurans* contains the conventional set

of DNA repair proteins found in non-radiation resistant organisms, some novel genes were identified (Makarova *et al*, 2001).

Tanaka *et al.*, 2004, monitored expression levels of genes in *D. radiodurans* following γ-irradiation by IR, as well as desiccation. The results showed that 72 genes were induced three-fold or more compared to basal expression levels following γ-radiation. Of the 72 genes up-regulated following γ-radiation, 33 were also expressed at elevated levels following desiccation.

The five genes whose expression is most highly induced in response to each stress include *ddrA, ddrB, ddrC, ddrD* and *pprA*. Interestingly, these genes are conserved in all *Deinococcus* spp. whose genomes have been sequenced, but are not found outside of the *Deinococcus* genus. Inactivation of these loci decreases viability upon exposure to IR (Zahradka *et* al., 2006).

Three of the genes were shown to play a major role in *D. radiodurans* radiation resistance (Tanaka *et al*., 2004). DdrA protects the ssDNA ends against degradation (Harris *et al*., 2004), whereas DdrB binds to ssDNA (Sugiman-Marangos and Junop, 2009) and facilitates SSA (Xu *et al*., 2011). PprA protects dsDNA ends against degradation and stimulates the activity of DNA ligases (Narumi *et al*., 2004), leading some to suggest the presence of a novel NHEJ-like pathway in *Deinococcus* spp. It is also interesting to note that three SOD and three catalase enzymes, which protect biomolecules from ROS-mediated damage, are induced after exposure to IR as well (Tanaka *et al*., 2004).

1.10 PROTEIN REGULATION IN RESPONSE TO RADIATION DAMAGE

The DNA damage response can also involve modulating protein function through post-translational modifications. Among these, phosphorylation is important for intracellular signaling in DNA damage repair (Sancar *et al*., 2004). Tyrosine phosphorylation of the SSB protein, for example, increases its activity nearly 200-fold (Mijakovic *et al*., 2006). In *D. radiodurans,* phosphorylation levels, ATP levels, and protein kinase activities are all increased following IR (Kamble *et al*., 2009). Elevated levels of protein phosphorylation were also found to attenuate nucleolytic activity in radiation-damaged *D. radiodurans* cells (Kamble *et al*., 2009).

Protein phosphorylation in response to radiation in *D. radiodurans* is mediated by a serine/threonine protein kinase (DR2518) (Rajpurohit *et al*., 2010) and by IrrE (PprI) (Lu *et al*., 2009). Although the target proteins and the regulatory pathways of the DR2518 protein kinase are yet to be identified, its physiological significance is reflected in the considerable radiation sensitivity of kinase-deficient *D. radiodurans* cells due to delayed DSB repair (Rajpurohit *et al*., 2010). Although global phosphorylation levels are increased, the level of serine/threonine phosphorylation decreases immediately after radiation damage in *D. radiodurans* (Rajpurohit *et al*., 2008). This indicates differential protein regulation in response to DNA damage depending on the type of phosphorylation modification.

1.11 PprA

Pleiotropic protein promoting DNA repair, PprA, was initially identified from a cosmid library as the gene responsible for DNA repair deficiency in a mutant strain of *D. radiodurans* (Narumi *et al*., 1997). This finding was complemented by transcriptional analysis (Liu *et al*., 2003) and subsequent knockout experiments (Tanaka *et al.,* 2004). PprA is unique to the *Deinococcus* genus, and is highly expressed following IR (Liu *et al*., 2003) and desiccation (Tanaka *et al*., 2004).

In vitro, PprA stimulates DNA end-joining reactions catalyzed by ATP- and NAD-dependent DNA ligases, while inhibiting *E. coli* exonuclease III activity, and may thus protect DNA ends from extensive degradation (Narumi *et al*., 2004). It binds DNA ends with a greater affinity than internal DNA regions and may even promote DNA looping (Murakami *et al*., 2006). The *pprA* mutant strain grows slower than the wild type. It is highly sensitive to IR, MMC (Narumi *et al*., 2004), and UV-A radiation (Bauermeister *et al*., 2009). A *pprA recA* double mutant is as sensitive to IR as the *recA* mutant, which suggests that PprA is epistatic to RecA. It would therefore appear that RecA and PprA function in the same pathway. PprA also stimulates *E. coli* catalase activity *in vitro*. By functioning similar to a Ku-like protein, PprA was proposed to stimulate NHEJ in *D. radiodurans* by the ATP-dependent ligase DRB0100 (Narumi *et al*., 2004). Although NHEJ has been suggested as a possible mechanism in DSB repair in *Deinococcus* spp., the

classical NHEJ mechanisms are inconsistent with the apparently error-free repair that has been reported in *Deinococcus*.

Most recently, PprA has been shown to be recruited onto the nucleoid following γ-irradiation (Devigne *et al*., 2013). Following this recruitment, PprA was shown to form a thread across the septum in dividing cells. This suggests PprA may play a crucial role in the control of DNA segregation and/or cell division following the completion of DNA DSB repair (Devigne *et al*., 2013).

1.12 PROPOSED ROLE OF PPRA IN *DEINOCOCCUS* DSB REPAIR

DNA repair in *Deinococcus* is currently thought to occur via two main pathways: SSA and ESDSA, which rely on cells containing an intact copy of the damaged DNA region.

Following fragmentation of genomic DNA, the shattered DNA fragments undergo 5' to 3' exonuclease resection, resulting in long ssDNA overhangs. These overhangs can anneal with complementary strands, yielding longer dsDNA fragments which can proceed into the ESDSA pathway.

DdrB plays an important role in SSA due to its single-stranded annealing activity (Xu *et al*., 2010; Sugiman-Marangos and Junop, 2013). DdrA may also be involved in protecting 3' ssDNA ends from degradation (Harris *et al*., 2009). Alternatively, DNA containing the 3' ssDNA overhangs can undergo RecA-mediated strand invasion of homologous duplexes and enter the ESDSA

pathway. After several subsequent rounds of extensive DNA synthesis by DNA Polymerase I and DNA Polymerase III, long pieces of linear dsDNA (up to 20 kb) are formed. These long dsDNA intermediates then undergo reassembly into complete genomic DNA via HR.

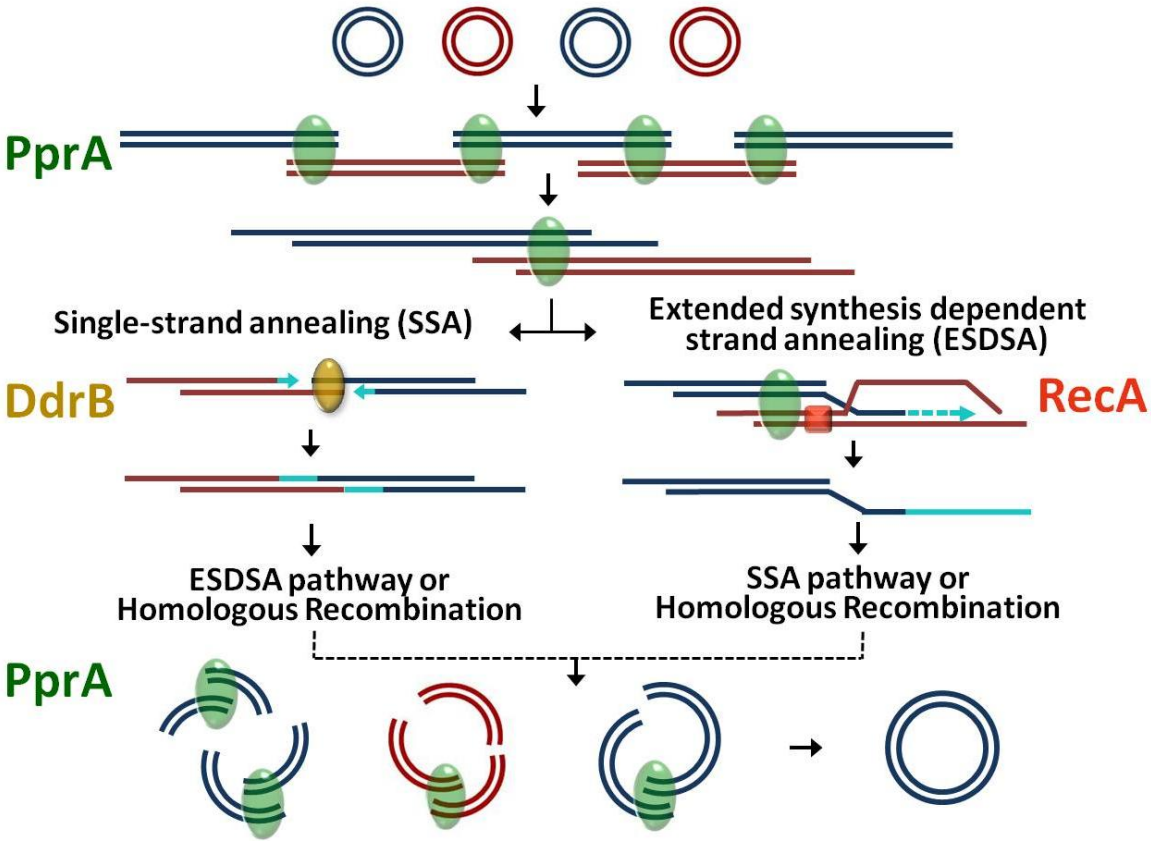

Figure 1.2 – Proposed model of DNA repair in *Deinococcus* spp. in response to extreme DSB damage with a focus on the speculated role of PprA in the DSB repair pathway. Repair is proposed to start with initial DSB recognition by PprA, followed by 5' to 3' resection of DNA ends (processing), single-strand annealing of complementary ssDNA overhangs, extensive DNA synthesis, and subsequent

reassembly of long linear pieces of duplex DNA to regenerate complete circular chromosomes via HR.

Based on the SSA and ESDSA repair pathways, PprA is proposed to be involved in the DSB repair by predominantly functioning in DNA bridging. This is based on the observation that PprA binds exclusively to dsDNA, and binds terminal DNA ends with a higher affinity than internal DNA regions (Murakami *et al*., 2006). PprA stimulates the DNA end-joining reaction catalyzed by ATP-dependent and NAD-dependent DNA ligases (Narumi *et al*., 2004), supporting its proposed involvement in the final reassembly of large circular chromosomes by HR.

1.13 PROJECT OBJECTIVES

At present, very little is known about how several key proteins, including PprA, function in DSB repair of *Deinococcus*. The goal of this work was to better understand the molecular mechanism(s) through which *Deinococcus* spp. are able to recover from severe DNA damage by characterizing the DNA binding activity of PprA, and further biochemically and structurally characterizing PprA.

Structure determination of PprA by X-ray crystallography was one avenue explored in an effort to gain functional insight. By solving the structure of PprA, valuable knowledge could be gained which would guide additional biochemical studies. To complement structural studies, unique properties of PprA were also characterized by transmission electron microscopy (TEM). With respect to these

unique properties, PprA was shown to form large fibrous filaments. Whether these filaments are essential to DNA repair remains to be determined.

Based on multiple sequence alignment, as well as secondary structure prediction models, various truncations of PprA from *D. radiodurans* were designed to guide further structural and biochemical characterization.

To explore the biological role that PprA plays in DSB repair, *in vivo* complementation studies were performed to test for recovery following severe DNA damage. Various truncations of PprA, as well as full-length protein were also complemented into a *Deinococcus* cells and tested for their ability to recover from severe DNA damage induced by exposure to UV radiation.

CHAPTER 2 – MATERIALS AND METHODS

CHAPTER 2. MATERIALS AND METHODS

2.1 CONSTRUCTS OF PPRA FROM VARIOUS *DEINOCOCCUS* SPP.

2.1.1 Full-length PprA from D. geothermalis

Expression vector MJ4602, full-length PprA from *D. geothermalis,* was constructed by Dr. Seiji Sugiman-Marangos. PprA from *D. geothermalis* was expressed as a His_6-MBP tagged protein.

2.1.2 Construct design and cloning of full-length PprA from D. radiodurans

Three full-length PprA expression vectors (MJ4812, MJ4813, and MJ4814) were generated by sub-cloning full-length *D. radiodurans* PprA, synthesized by GeneArt® (http://www.geneart.com/), into pDEST527, pDEST-HisMBP, and pDEST565 respectively, creating TEV-cleavable His_6, His_6-MBP and His_6-GST tagged constructs.

2.1.3 Construct design and cloning of N- and C-terminal truncations of PprA from D. radiodurans

D. radiodurans PprA N-terminal truncations $PprA_{9-284}$, $PprA_{40-284}$ and $PprA_{56-284}$ (MJ4940, MJ4941, and MJ4942, respectively) and C-terminal truncations $PprA_{1-242}$, $PprA_{1-218}$ and $PprA_{1-170}$ (MJ4943, MJ4944, and MJ4945, respectively) were created by PCR-amplifying the desired PprA fragments and cloning them into a pET28-MHL vector by ligation independent cloning (LIC), creating TEV-cleavable His_6 fusions. These same truncations were also

generated by PCR-amplifying the desired PprA fragments and cloning into pDEST-HisMBP and pDEST544 using Gateway® technology (Invitrogen), creating TEV-cleavable His_6-MBP and His_6-NusA tagged constructs.

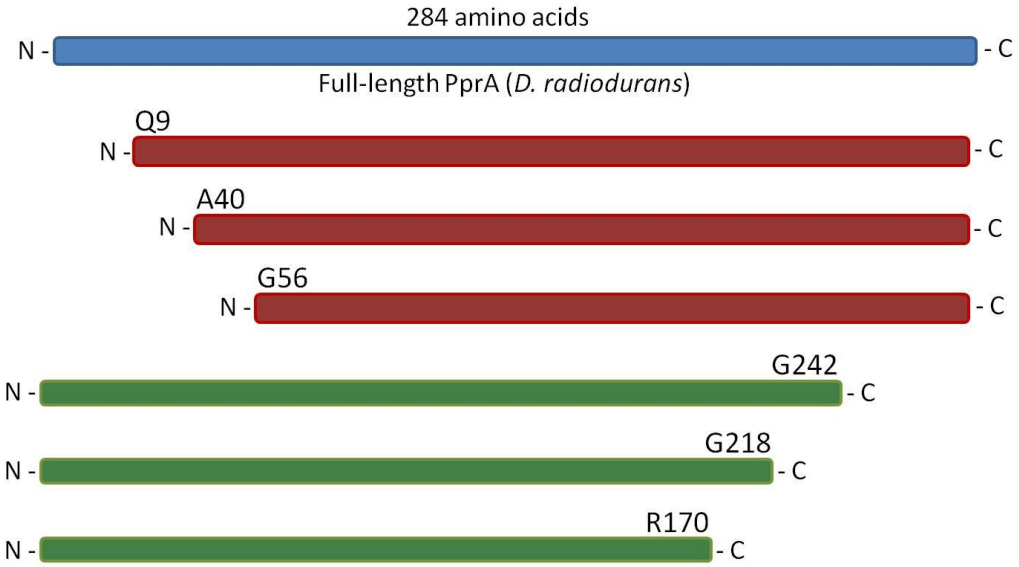

Figure 2.1 – Design of N-terminal (red) and C-terminal (green) truncations of PprA from *D. radiodurans*. Truncations were designed based on multiple sequence alignment (Appendix B) and secondary structure prediction models (Appendix D).

2.1.4 Construct design and cloning of full-length PprA from D. proteolyticus, D. deserti, D. gobiensis and D. maricopensis

Full-length PprA genes from four homologs of *D. radiodurans* were obtained from GenScript (http://www.genscript.com/), with *attB1* and *attB2*

recombination sites, in a pUC57 vector conferring kanamycin resistance. The full-length PprA genes from *D. proteolyticus, D. deserti, D. gobiensis,* and *D. maricopensis* were cloned into pDEST527 and pDEST-HisMBP expression vectors using Gateway® technology (Invitrogen), to generate TEV-cleavable His_6 and His_6-MBP tagged constructs.

2.2 PROTEIN EXPRESSION

2.2.1 Protein expression of full-length PprA from D. geothermalis

Full-length PprA (32.7 kDa) from *D. geothermalis* was expressed in *E. coli* BL21(DE3) cells under the control of the T7 RNA polymerase promoter as an N-terminal His_6-MBP (43.9 kDa) tagged fusion protein. A 10 mL overnight culture was used to inoculate 1 L of LB containing 100 μg/mL ampicillin. Bacterial cultures were grown at 37°C with shaking at 225 RPM, to an optical density at 600 nm (OD_{600}) of ~0.5, and induced with 1 mM isopropyl β-D-thiogalactopyranoside (IPTG) for 3 h. Cells were harvested by centrifugation at 4000 x g, frozen in liquid nitrogen (LN_2) and stored at -80°C.

2.2.2 Protein expression of PprA from D. radiodurans

PprA proteins (full-length PprA, $PprA_{1-242}$, $PprA_{1-218}$, $PprA_{1-170}$, $PprA_{9-284}$, $PprA_{40-284}$, $PprA_{56-284}$) from *D. radiodurans* were expressed in *E. coli* BL21(DE3) cells as N-terminal His_6-MBP or N-terminal His_6-NusA tagged fusion proteins. A 10 mL overnight culture was used to inoculate 1 L of LB containing 100 μg/mL

kanamycin. Bacterial cultures were grown at 37°C with shaking at 225 RPM, to an OD_{600} of ~0.5, and induced with 1 mM IPTG for 3 h. Cells were harvested by centrifugation at 4000 x g, frozen in LN_2 and stored at -80°C.

2.2.3 Protein expression of PprA from D. peraridilitoris

Full-length PprA from *D. peraridilitoris* was expressed in *E. coli* BL21(DE3) cells as an N-terminal His_6-MBP tagged fusion protein. A 10 mL overnight culture was used to inoculate 1 L of LB containing 100 μg/mL ampicillin. Bacterial cultures were grown at 37°C with shaking at 225 RPM, to an OD_{600} of ~0.5, and induced with 1 mM IPTG for 3 h. Cells were harvested by centrifugation at 4000 x g, frozen in LN_2 and stored at -80°C.

2.3 PROTEIN PURIFICATION

2.3.1 Protein purification of full-length PprA from D. geothermalis

An induced cell pellet (described in *2.2.1*) was resuspended in lysis buffer (20 mM Tris pH 8.0, 800 mM NaCl, 5 mM imidazole), and protease inhibitors (PMSF, benzamidine, pepstatin A, leupeptin, and aprotonin A) were added to a final concentration of 1 mM. The resuspended pellet was lysed by French Press (3 passes at 20,000 psi), and protease inhibitors were added again, to a final concentration of 1 mM. Following lysis, the sample was clarified by centrifugation (40 min, 40,000 x g, 4°C). Following filtering, the His_6-MBP-PprA (~76 kDa) sample was loaded onto a 5 mL Ni immobilized metal affinity chromatography

(IMAC) column (GE Healthcare Life Sciences) at 0.5 mL/min using an ÄKTA FPLC (GE Healthcare Life Sciences).

The bound protein was washed with ≥100 mL wash buffer (95 mM imidazole) prior to elution (500 mM imidazole). Ni-IMAC column eluate was exchanged into low salt buffer (20 mM Tris pH 8.0, 50mM NaCl) prior to cleavage of the His_6-MBP fusion tag with TEV protease. Cleaved His_6-MBP fusion tag, and TEV were separated from PprA by ion exchange chromatography using a Q-sepharose column (GE Healthcare Life Sciences), and PprA was then concentrated to ~2 mg/mL by ultrafiltration centrifugation.

2.3.2 Protein purification of $PprA_{25-300}$ from D. radiodurans

An induced pellet (described in *2.2.2*) was resuspended in lysis buffer (20 mM Tris pH 8.0, 800 mM NaCl, 5 mM imidazole), and protease inhibitors (PMSF, benzamidine, pepstatin A, leupeptin, and aprotonin A) were added to a final concentration of 1 mM. The resuspended pellet was lysed by French Press (3 passes at 20,000 psi), and protease inhibitors were added again, to a final concentration of 1 mM. Following lysis, the sample was clarified by centrifugation (40 min, 40,000 x g, 4°C). Following filtering, His_6-$PprA_{9-284}$ (~30 kDa) was loaded onto a 5 mL Ni-IMAC column at 0.5 mL/min using an ÄKTA FPLC (GE Healthcare Life Sciences). The bound protein was washed with ≥100 mL wash buffer (95 mM imidazole) prior to elution (500 mM imidazole).

2.3.3 Protein purification of full-length PprA from D. peraridilitoris

An induced cell pellet (described in *2.2.3*) was resuspended in lysis buffer (20 mM Tris pH 8.0, 800 mM NaCl, 5 mM imidazole), and protease inhibitors (PMSF, benzamidine, pepstatin A, leupeptin, and aprotonin A) were added to a final concentration of 1 mM. The resuspended pellet was lysed by French Press (3 passes at 20,000 psi), and protease inhibitors were added again, to a final concentration of 1 mM. Following lysis, the sample was clarified by centrifugation (40 min, 40,000 x g, 4°C). Following filtering, the His_6-MBP-PprA (~76 kDa) sample was loaded onto a 5 mL Ni-IMAC column (GE Healthcare Life Sciences) at 0.5 mL/min using an ÄKTA FPLC (GE Healthcare Life Sciences).

The bound protein was washed with ≥100 mL wash buffer (95 mM imidazole) prior to elution (500 mM imidazole). Ni-IMAC column eluate was diluted by a factor of 4 to decrease the NaCl concentration to 200 mM, and imidazole concentration to 125 mM imidazole, prior to cleavage of the His_6-MBP fusion tag with TEV protease. Following cleavage, the salt concentration was increased to 800 mM NaCl, and the solution was buffer exchanged back into the original lysis buffer. PprA was recovered by reverse Ni-IMAC chromatography using a gradient from 5 mM imidazole to 153.5 mM imidazole (0.5 mL/min, 180 min). Fractions containing PprA were pooled and placed in 10,000 MWCO dialysis tubing, buried in PEG 35,000 until the volume decreased, reaching a final protein concentration of ~2 mg/mL.

2.4 ELECTRON MICROSCOPY (EM)

2.4.1 Buffer exchange into EM buffer

Protein samples were buffer exchanged into electron microscopy (EM) buffer (10 mM Tris pH 8.0, 150 mM NaCl) using a 10,000 MWCO Slide-A-Lyzer MINI dialysis device (Thermo Scientific).

2.4.2 Negative staining

Samples for EM studies were prepared on freshly made continuous carbon grids – copper, 400 mesh (Electron Microscopy Science). EM grids were glow discharged in air for 30 s (Aebi and Pollard 1987). EM grids were floated on a 5 μL drop of protein solution (50-150 μg/mL) for 2 min. Excess sample was blotted off against filter paper (Whatman®) and the grids were stained with 1% (w/v) uranyl acetate solution for 1 min, blotted, and air-dried thoroughly. The 1% (w/v) uranyl acetate solution was prepared fresh, in water. The stain solution was filtered with Acrodisc 25 mm syringe filter with 0.2 mM Supor Membrane (PALL Corporation) before use.

2.4.3 Transmission Electron Microscopy (*TEM*)

Negative stained EM grids were visualized at a nominal magnification of 100,000 X in a JEOL JEM 1200 TEMSCAN (JEOL, Peabody, MA, USA) operating at an accelerating voltage of 80 kV. All images were acquired on an AMT XR-41 Side-Mount cooled 4 megapixel format CCD camera (Advanced

Microscopy Techniques Corp., Danvers, MA, USA). AmtV600 software was used to capture digital images.

2.5 ELECTROPHORETIC MOBILITY SHIFT ASSAY (EMSA)

DNA binding experiments were performed in electrophoretic mobility shift assay (EMSA) buffer (10 mM Tris pH 7.6, 10 mM $MgCl_2$, 1 mM dithiothreitol and 50mM NaCl), carried out in 20 μL reactions containing 50 ng DNA and varying concentrations of protein. Binding reactions were incubated for 30 min at 37°C then subjected to gel electrophoresis on either a 6% polyacrylamide native TBE gel (100 V for 1.5 h) or a 1% agarose gel (100 V for 40 min), depending on the size of DNA substrate used.

2.6 GEL FILTRATION CHROMATOGRAPHY

Gel filtration experiments were performed using an ÄKTA FPLC (GE Healthcare Life Sciences) on a Superdex 200 column (GE Healthcare Life Science) pre-equilibrated with 20 mM Tris pH 8.0, 800 mM NaCl. The column was run at a flow rate of 0.5 mL/min. Elution profiles were monitored with an in-line UV-900 detector at λ = 280 nM. Eight proteins of known molecular weight (thyroglobulin 669 kDa, ferritin 440 kDa, catalase 232 kDa, aldolase 158 kDa, albumin 67 kDa, ovalbumin 43 kDa, chymotrypsinogen 25 kDa, ribonuclease A 13.7 kDa) were used as standards to calibrate the column. The molecular weight of sample proteins was determined using a logarithmic curve of the molecular weight plotted against V_e/V_o.

2.7 CRYSTALLIZATION AND X-RAY DIFFRACTION DATA

2.7.1 Crystallization

All crystallization trials of PprA were performed at either 20°C or 4°C using the hanging-drop vapour-diffusion method. Equal volumes (1 μL) of protein (1-2 mg/mL) and crystallization condition were mixed and suspended over 0.5 mL 1.5 M $(NH_4)_2SO_4$ solution. Where applicable, additive conditions were introduced to the drop at a final concentration of 10% v/v (0.2 μL).

2.7.2 X-ray Diffraction Data Collection

Crystals of full-length PprA from *D. geothermalis*, grown in 1.0 M ammonium phosphate dibasic, 0.1 M imidazole:HCl, 40% v/v pentaerythritol ethoxylate, were mounted and exposed for 2 seconds in 1° increments at a wavelength of 0.9791 Å. X-ray diffraction data was collected at the National Synchrotron Light Source (NSLS) X25 beamline at Brookhaven National Laboratory. The data was processed and scaled with HKL2000 to 8 Å.

2.8 *IN VIVO DEINCOCCUS* SURVIVAL ASSAY

2.8.1In vivo Characterization of PprA

D. radiodurans strains TNK105 (Δ*pprA*) and GY14615 (pprA::HA/kan) were generously provided by Dr. John Battista (Louisiana State University) and by Dr. Pascale Servant (Université Paris-Sud), respectively. A complementation

plasmid expressing the *groESL* operon under the control of its native promoter (pRADZ3) was generously provided by Dr. Mary Lidstrom (University of Washington).

The *pprA* gene from *D. radiodurans* was PCR-amplified, incorporating the native radiation responsive promoter in the primer design (Table 1). The gene was sub-cloned into a pJET1.2 vector using the CloneJET kit (Thermo Scientific), following the manufacturer's protocol, before cloning into the pRADZ3 *Deinococcus* shuttle vector at the BglII and XbaI restriction sites. Four N- and C-terminal deletions of PprA (ΔQ9, ΔA40, ΔG242 and ΔR170) were introduced into the pRADZ3 *Deinococcus* shuttle vector in the same manner.

Table 1. Sequence of the radiation responsive promoter of the *D. radiodurans pprA* gene

5'-TATGCCAGAGTGCTACCCCTGGCCTTTTTAATCTGTTCAGGGCATAATAAAGGCAGT-3'

Cloning of the two outstanding PprA truncations described previously in *2.1.3* was unsuccessful, despite several attempts to generate a ligated product. The *Deinococcus* shuttle vectors containing *pprA* genes of interest were transformed into competent PprA knockout strains (TNK105), following the transformation protocol described by Bouthier de la Tour *et al*., 2011.

2.8.2 Plating assay monitoring cell survival post-UV exposure

A plating assay to monitor cell survival following exposure to 254 nm UV-C was developed.

Overnight cultures of *D. radiodurans* TNK105 complemented with various versions of *pprA* were grown in 1X TGY (0.5% Bactotryptone, 0.1% Glucose, 0.3% Yeast Extract) to an OD_{600} between 0.5-1.5, before diluting to an OD_{600} of ~0.1 (representative of early exponential growth phase). 1/10; $1/10^2$; $1/10^3$; $1/10^4$ and $1/10^5$ dilutions were prepared, and 10 μL of each dilution were plated on TGY agar. Using an LMS-20E UV transilluminator (UVP®), plates were exposed to 254 nm UV-C radiation for varying amounts of time. Exposure was measured using a hand-held Model 8.0 UVC Radiometer (Solartech Inc.) Following UV-irradiation, cells were grown at 30°C for 36-54 h to allow for recovery.

2.8.3 Dominant negative effect of PprA truncations in WT D. radiodurans cells

The *Deinococcus* shuttle vectors containing *pprA* genes of interest were transformed into competent WT *D. radiodurans* cells. To test whether an inability to recover from UV-induced DNA damage in the complemented knockout *D. radiodurans* strain would be observed when PprA truncations were introduced into a WT *D. radiodurans* strain. Termed 'dominant-negative' effects, these experiments examined whether the negative effect of the truncated proteins, resulting in the inability of *D. radiodurans* to recover from UV-induced DNA damage was dominant over the typically observed phenotype of WT *D.*

radiodurans, which can readily recover from identical exposure levels of UV-radiation.

CHAPTER 3 – RESULTS

CHAPTER 3. RESULTS

3.1 PURIFICATION OF PPRA

PprA was purified several times over the course of this project to obtain high levels of protein for use in both structural and functional studies. A representative purification of PprA from *D.* radiodurans is shown in Figure 3.1.

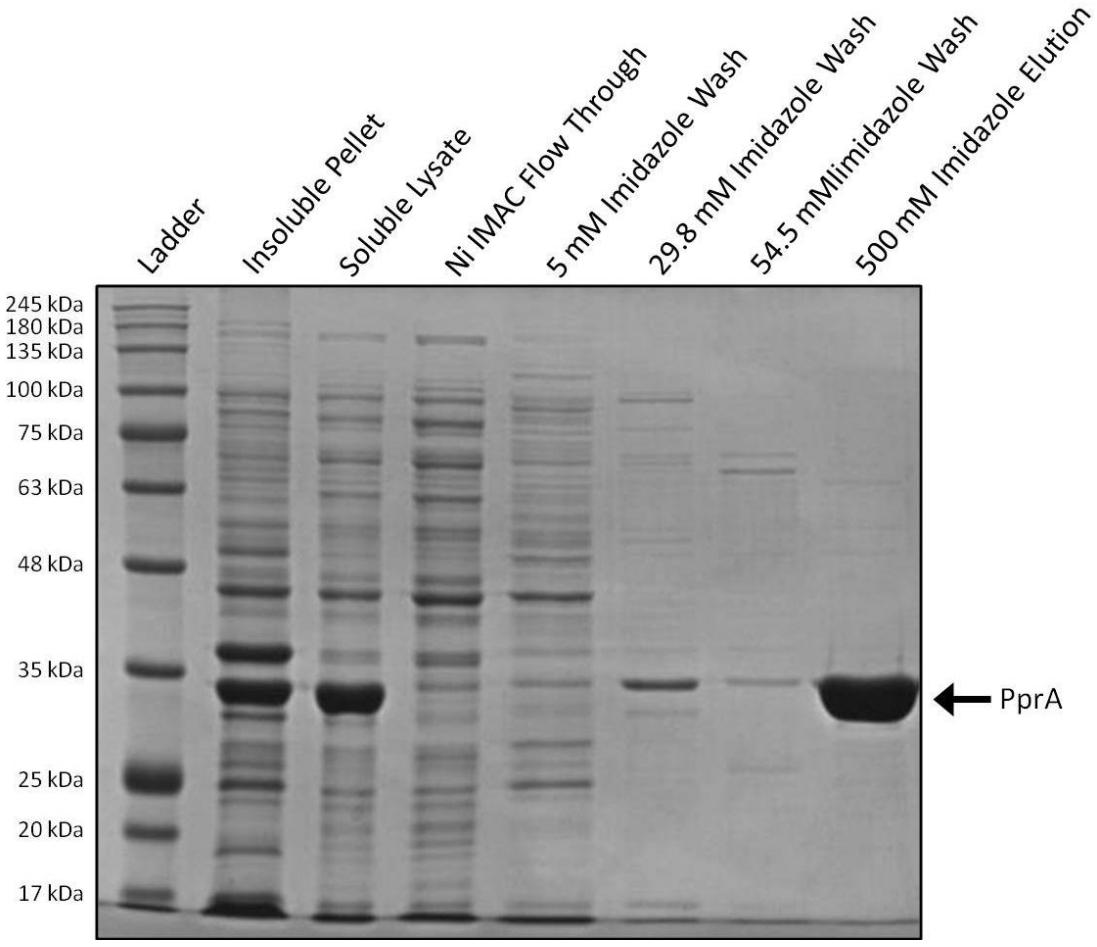

Figure 3.1 – 12% SDS-PAGE gel showing the purification of $PprA_{9-284}$ from *D. radiodurans*. PprA was purified using Ni-IMAC, and elutes as a near homogeneous protein.

PprA was expressed in *E. coli* BL21(DE3) cells as a hexa-histidine (His_6) N-terminal fusion. Certain versions of PprA (i.e. from *D. geothermalis, D. peraridilitoris,* and various truncations of PprA from *D. radiodurans*) were expressed with additional fusion protein tags, for the purpose of generating soluble protein.

Of the various protein constructs of PprA described in this thesis, the $PprA_{9-284}$ N-terminal truncation from *D. radiodurans* was both the most soluble, and highest yielding construct. As such, the majority of the DNA binding studies, EM experiments and gel filtration studies were conducted using the $PprA_{9-284}$ protein.

To obtain a highly pure sample of PprA, the protein was purified using Ni^{2+}-charged resin to trap the His_6-tagged protein. To maximize protein purity, extensive washes (≥ 100 mL) were performed at various concentrations of imidazole (5 mM, 29.75 mM, and 54.5 mM) to remove protein impurities. The final elution contained highly pure, near homogeneous PprA protein, which migrated on a 12% SDS-PAGE gel between the 25 and 35 kDa markers. Figure 3.1 depicts an SDS-PAGE gel representative of a typical purification of $PprA_{9-284}$ from *D. radiodurans.*

To assess the presence of DNA contamination resulting from co-purification with protein, ratios of absorption at 260 nm versus 280 nm were determined. $Abs_{260:280}$ were consistently between 0.60 and 0.80, suggesting

minimal, to no nucleic acid contamination in the protein samples. Furthermore, protein purifications were carried out at very high salt concentrations (800 mM NaCl), which reduces electrostatic interactions and prevents co-purification of nucleic acids with protein.

3.2 DNA BINDING STUDIES OF PPRA

Following purification of PprA, it was necessary to confirm that the purified protein was active. This was done by performing DNA binding assays to not only verify activity, but also further characterizing functional and biochemical aspects of the protein.

To investigate the DNA binding activity of PprA, electrophoretic mobility shift assays (EMSAs) were performed (Figure 3.2). PprA from both *D. geothermalis*, as well as *D. radiodurans*, was shown to bind exclusively to linear dsDNA (Figure 3.2). As PprA was titrated into EMSA reactions (0 μM, 5 μM, 12.5 μM, 16.7 μM), the movement of the pUC19 band was observed and the presence of a gel shift confirmed binding. The presence of a smear on the gel suggested the presence of multiple binding sites. As shown in the bottom EMSAs (Figure 3.2), PprA was unable to bind nicked or circular DNA, as evidenced by a lack of a shift of the pUC19 band.

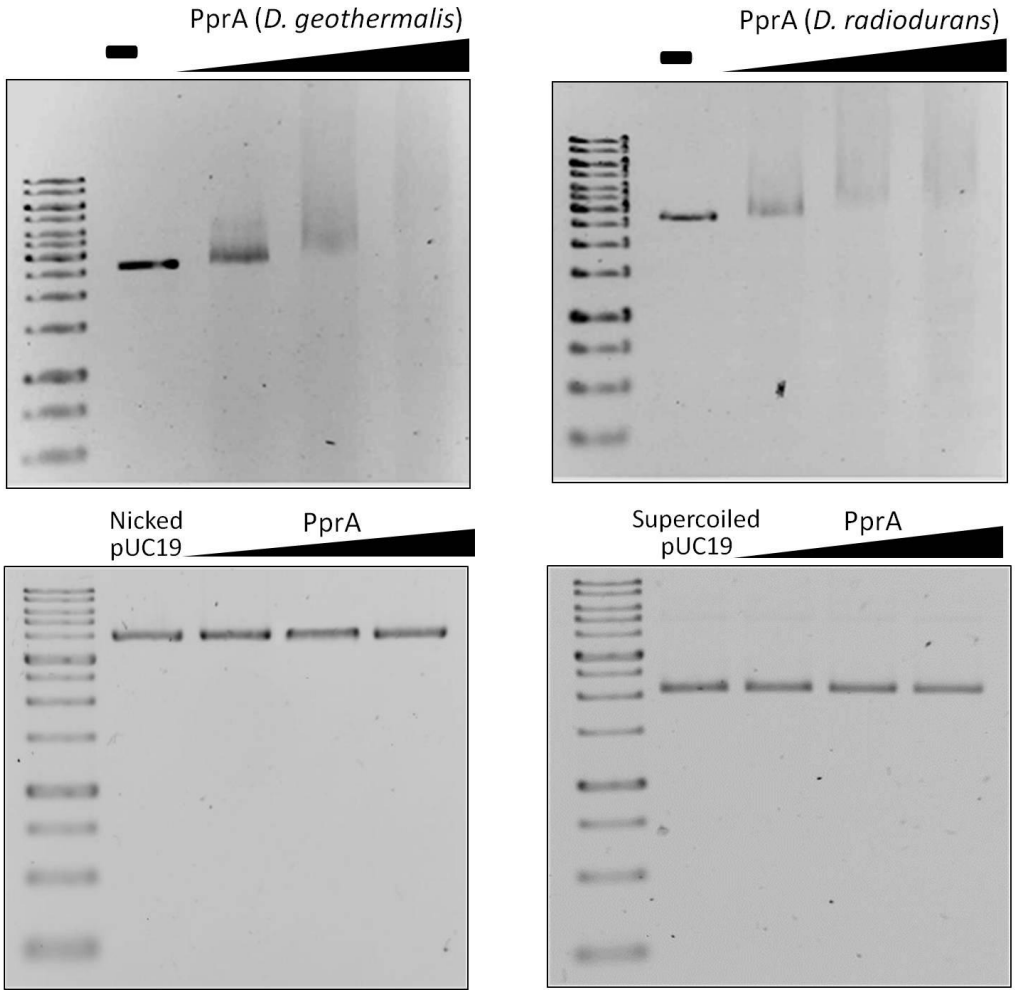

Figure 3.2 – EMSA of PprA with various dsDNA substrates (pUC19). PprA demonstrated the ability to shift linear dsDNA, but was unable to bind nicked or supercoiled DNA.

These EMSA experiments suggested the need for a freely accessible DNA end, such as one that would be generated as a result of a DSB. This observation supported the proposed role of PprA as an end-binding DNA DSB recognition factor.

To further characterize the DNA binding length specificity of PprA, EMSAs were performed using a DNA ladder as a substrate in binding reactions (Figure 3.3).

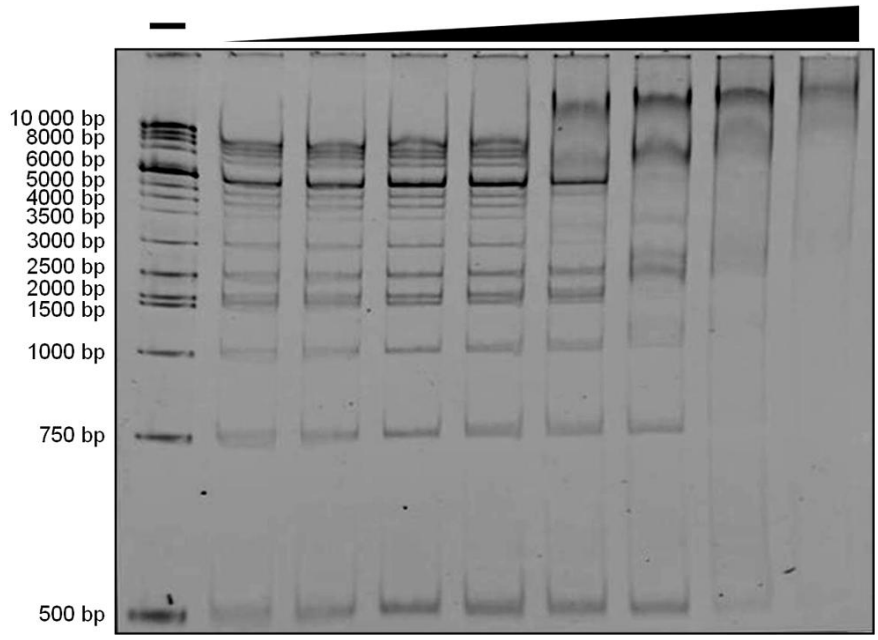

Figure 3.3 – EMSA characterizing the binding of $PprA_{9-284}$ from *D. radiodurans* with different sizes of linear dsDNA using a 1 kb ladder as a DNA substrate. Increasing amounts of PprA (0.14 μM, 0.27 μM, 0.54 μM, 1.1 μM, 2.2 μM, 4.4 μM, 8.8 μM, and 17.5 μM) were titrated into the EMSA binding reaction. EMSA products were resolved on a 6% native PAGE run at 100 V for 1.5 h.

At protein concentrations of ≤ 1.1 μM PprA, there were no detectable band shifts. At a concentration of 2.2 μM PprA, higher molecular weight bands were shifted, confirming the DNA binding activity of PprA. At this concentration of protein, PprA bound to dsDNA 3500-4000 bp in length.

Therefore, PprA binds longer pieces of dsDNA (≥3500-4000 bp) with a higher preference than shorter pieces of dsDNA (≤1000 bp).

3.3 GEL FILTRATION STUDIES OF PPRA

To characterize the oligomeric state of PprA, size exclusion chromatography experiments were performed, which showed that PprA elutes in the void volume of an S200 gel filtration column (Figure 3.4). These data provide evidence that PprA forms a large multimer in solution, or has an unusually elongated shape with a large Stokes radius.

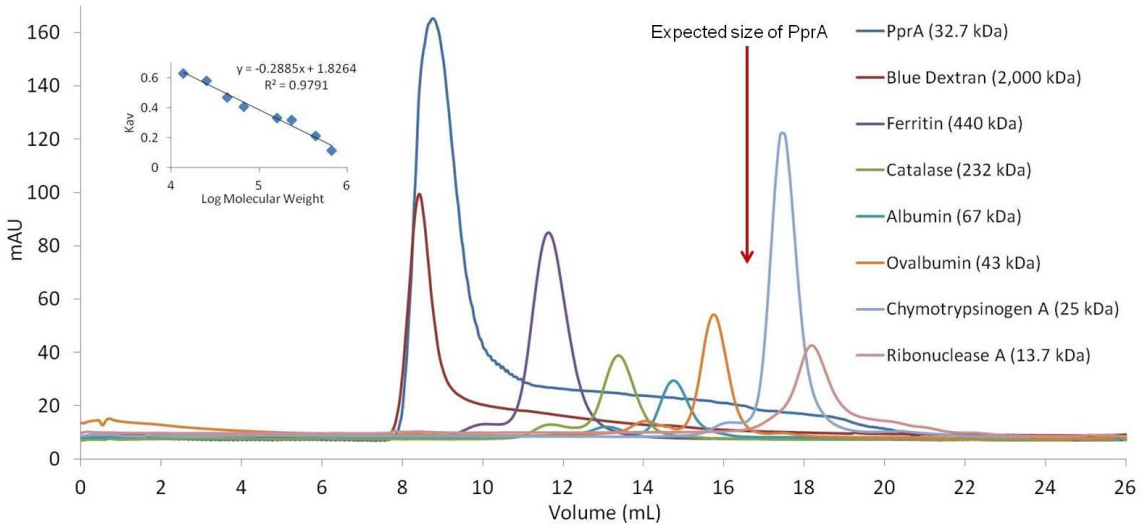

Figure 3.4 – The elution profiles of seven proteins of known molecular weight were run as standards to calibrate the S200 gel filtration column. Based on its predicted mass, PprA (~32 kDa) was expected to elute after ovalbumin (43 kDa), but before chymotrypsinogen A (25 kDa), however, PprA eluted in the void volume.

Although PprA eluted in the void volume, it was notable that there was a significant amount of 'tailing' occurring. This phenomenon was observed as a prolonged shoulder with a gradual drop off in absorbance, before returning to the true baseline value. This behaviour suggests multiple species of PprA exist in solution, with the predominant species forming a large multimeric complex.

3.4 FILAMENT FORMATION *IN VITRO*

One of the earliest observations made when working with PprA was the viscous nature of the cell lysate during the purification of the protein. In addition to the viscosity of the cell lysate, the protein was observed to elute from an S200 gel filtration column in the void volume (Figure 3.4), suggesting a very large structure in solution. Based on these observations, electron microscopy (EM) was used to visualize and characterize the protein.

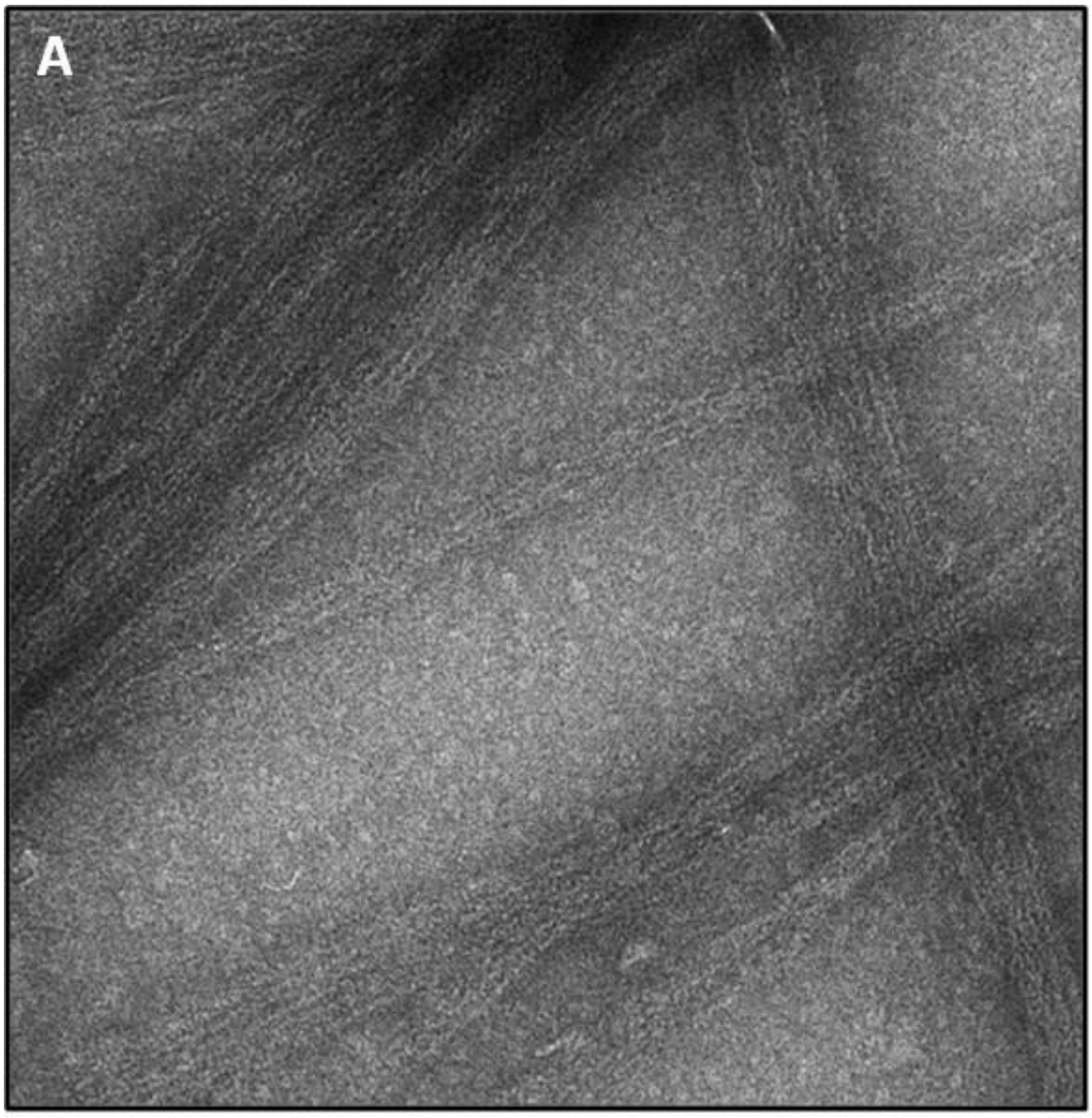
A
D. geothermalis
100 nm

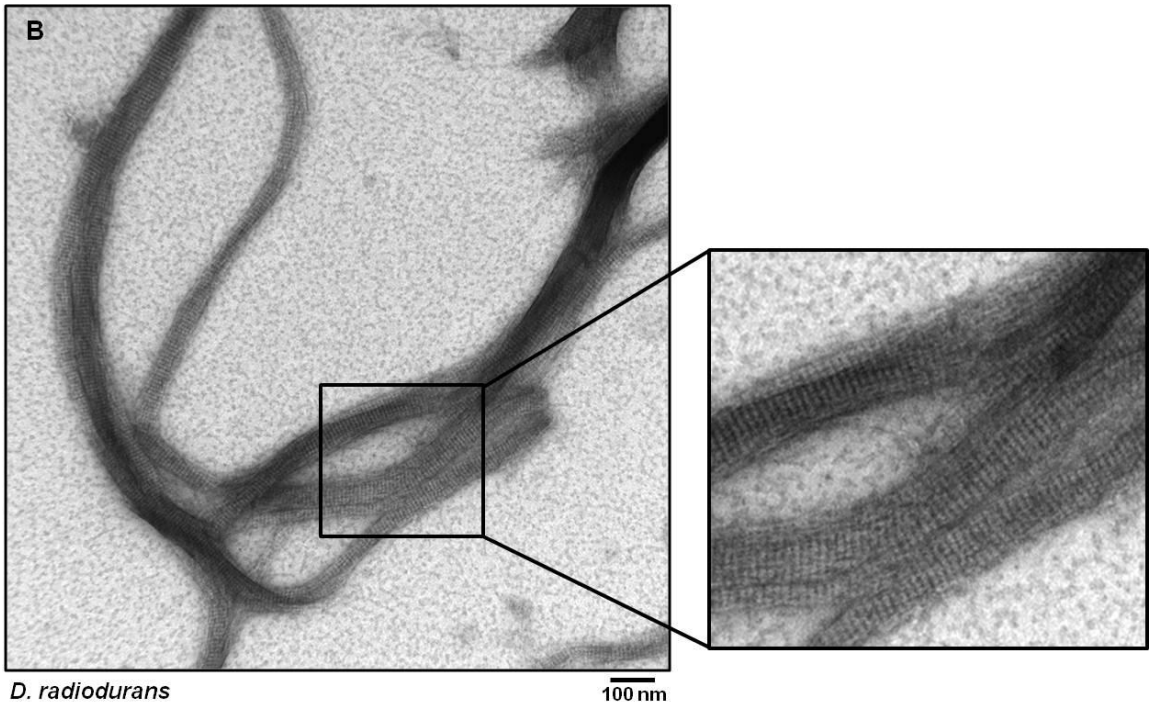
B
D. radiodurans
100 nm

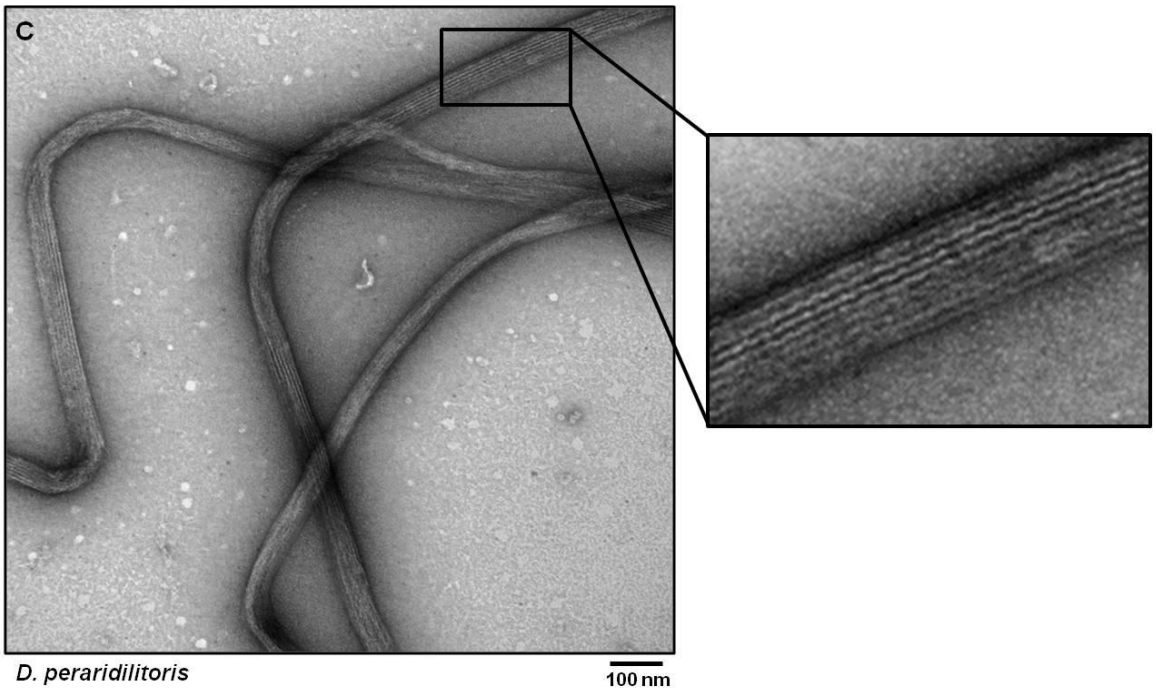
C
D. peraridilitoris
100 nm

Figure 3.5 – EM micrographs of purified PprA revealed that PprA forms a large network of protein filaments. Long filaments of PprA from *D. geothermalis* (A), *D. radiodurans* (B), and *D. peraridilitoris* (C) were observed. Images were viewed at 100,000 X magnification. Inset images show enlarged filament segments.

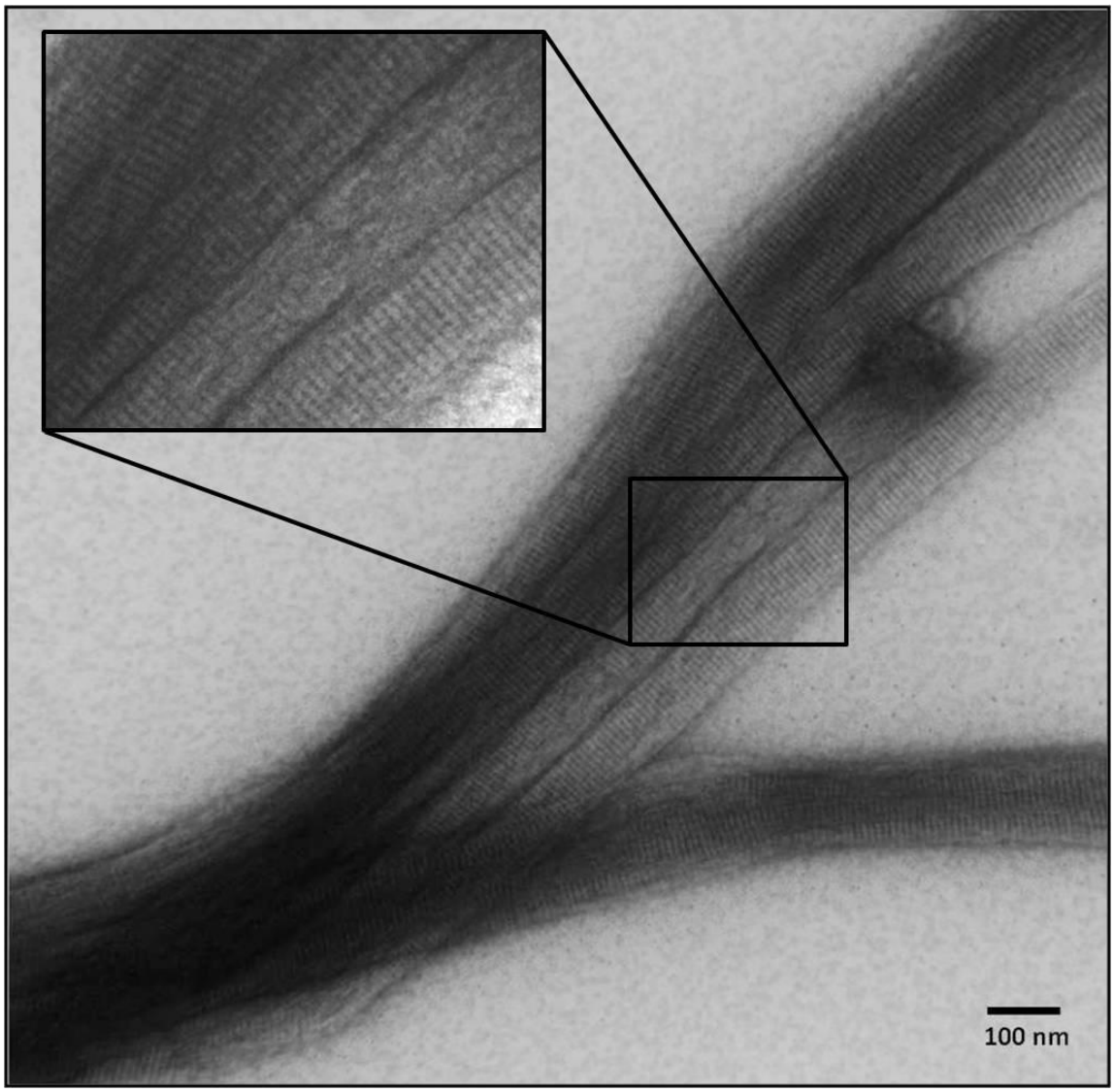

Figure 3.6 – TEM micrograph of a *D. radiodurans* PprA filament bundle visualized at 200,000 X magnification. Inset is an enlarged image of the filament.

An important question is whether these filaments are important for PprA function in DNA repair and radiation resistance. The observation that PprA filaments are conserved between three different *Deinococcus* spp. strongly suggests the filaments have some biological role.

The filaments from all three species self-organized into higher order structures and filament bundles. These structures are highly reminiscent of those formed by XLF, an important repair factor implicated in DNA end-binding (like Ku 70/80), bridging and stimulation of DNA ligase in the NHEJ pathway. In the case of XLF, filaments formed more readily in the presence of DNA. In the case of PprA however, filaments formed in the absence of DNA (Figure 3.7).

A glycine to glutamic acid substitution at amino acid position 149 in PprA from *D. radiodurans* abolished DNA binding activity (Narumi *et al*., 2004). To test whether filament formation was related to DNA binding activity, site-directed mutagenesis was performed to generate a DNA-binding deficient mutant of PprA from *D. radiodurans*. EMSA experiments with the $PprA_{9-284}$ G149E mutant confirmed that the mutant does not bind DNA.

Interestingly, the DNA binding mutant $PprA_{9-284}$ G149E formed filaments indistinguishable from the wild type. Based on this result, it would appear that filament formation is not dependent on DNA binding.

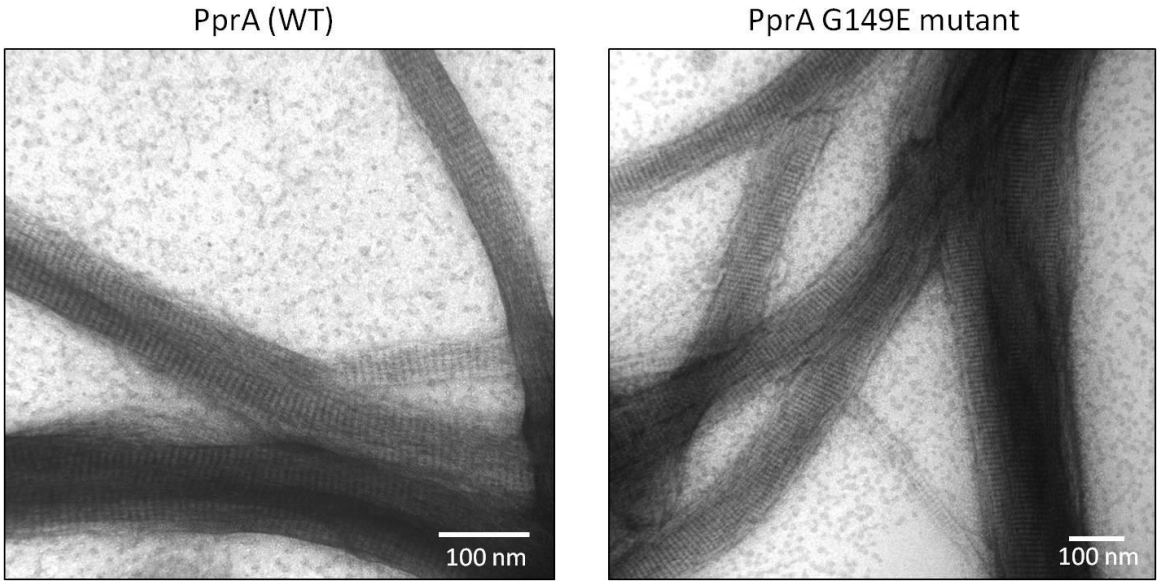

Figure 3.7 – DNA binding is not required for filament formation, as a DNA-binding mutant, G149E, forms filaments similarly to the wild type. The DNA-binding mutant was confirmed to not bind linear dsDNA using EMSA (data not shown).

In order to further characterize PprA and determine whether filaments play a role in DSB repair, a filament disrupting mutant, which still bound DNA, had to be identified. To search for filament disrupting mutants, the sequences and structures of XLF and XRCC4 (Andres and Junop, 2011; Andres *et al*., 2012) were used to identify potential sites that might disrupt filament formation. In analyzing the sequence and structure of XRCC4 and XLF, several amino acid residues were identified that could be expected to prevent filament assembly if PprA and XRCC4/XLF have structural homology. These include K99, K65, D58 and F106 in XRCC4, and L115, L65, R64 and E111 in XLF. Based on this

information, the secondary structure prediction model of PprA was analyzed for exposed hydrophobic residues found in loop or turn regions between predicted α-helices (Appendix D).

Three mutations were generated using site-directed mutagenesis; $PprA_{9-284}$ L164D, $PprA_{9-284}$ F165D, and $PprA_{9-284}$ V166D.

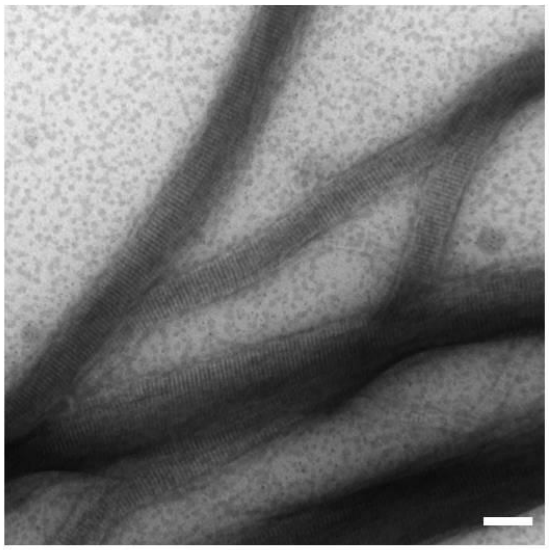

$PprA_{9-284}$ L164D

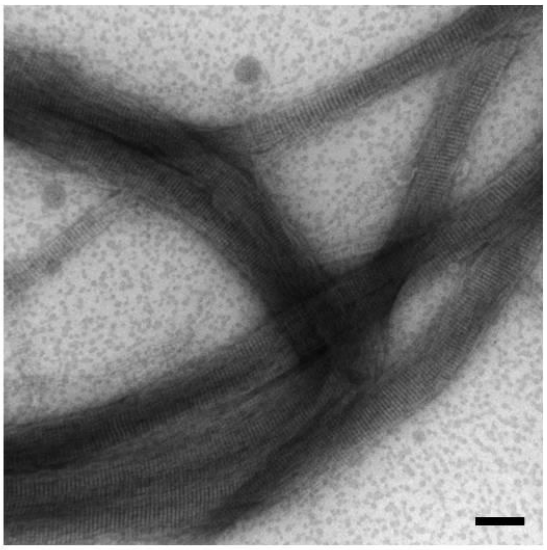

$PprA_{9-284}$ F165D

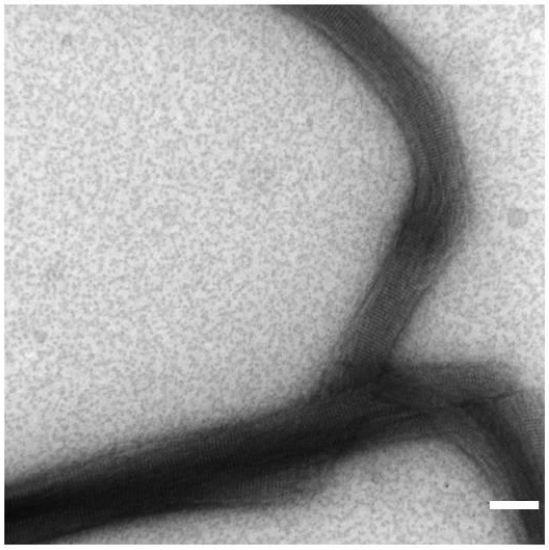

$PprA_{9-284}$ V166D

Figure 3.8 – A search for filament disrupting mutants of PprA based on XLF and XRCC4 sequence and structure. Three unique point mutations (L164D, F165D and V166D) did not abolish filament formation in $PprA_{9-284}$ from *D. radiodurans*. The filament morphology is similar, including striations. Scale bars represent 100 nm.

3.5 SALT-DEPENDENCY OF PPRA FILAMENTS

Filament formation was initially thought to be salt dependent, and that filament formation could be disrupted with high salt concentrations. Studies to determine the relationship between filament formation and salt concentration however revealed that filaments persisted at concentrations of 200mM, 400mM, 800mM, 1200mM and 1600mM NaCl. Thus, filament formation cannot be fully disrupted by increasing ionic strength.

3.6 CRYSTALLIZATION OF FULL-LENGTH PPRA FROM *D. GEOTHERMALIS*

PprA from various *Deinococcus* spp. were pursued as targets in crystallographic studies. Full-length PprA from *D. geothermalis* was screened against several crystallization kits, including Nextal Classics (QIAGEN), Emerald, Wizard™ I, Wizard™ II (Emerald Bio), The Joint Center for Structural Genomics (JCSG) core suite I, II, III and IV (QIAGEN), and the Midwest Center for Structural Genomics (MCSG) core suite I, II, III and IV (Microlytic).

Crystals grew in several different conditions from several different screens (Table 3; Appendix A), however those from MCSG III – condition #4 produced the most promising crystals. Crystals generated in this condition resulted from drops with a high degree of nucleation, lacking background precipitation. Crystals varied in initial size, suggesting the potential for further growth. Initial attempts to crystallize PprA from *D. geothermalis* however, yielded small, needle-like crystals.

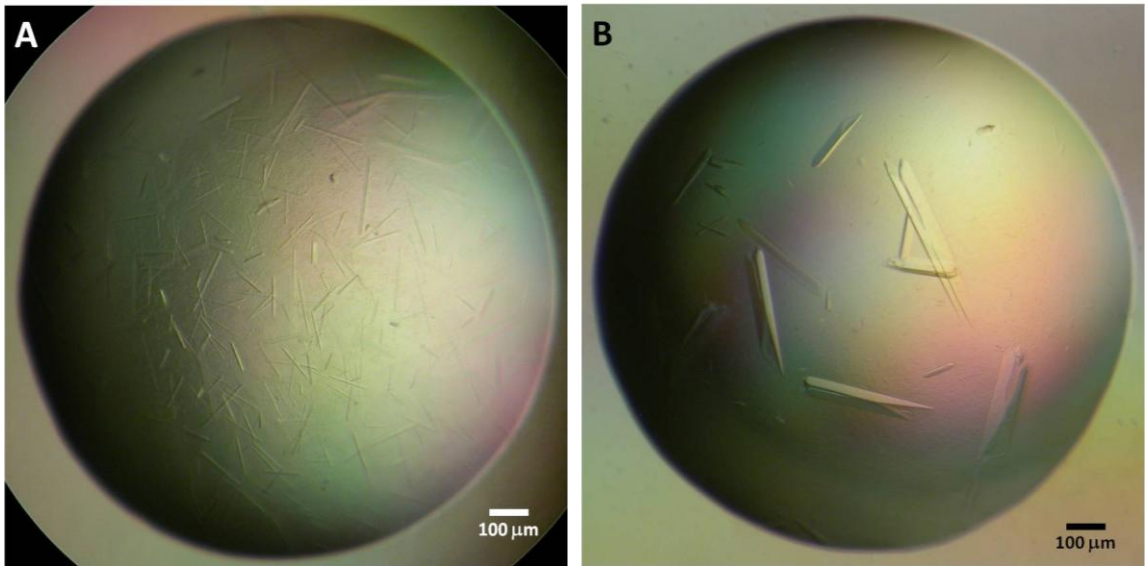

Figure 3.9 – Crystals of full-length PprA from *D. geothermalis* grown with Midwest Center for Structural Genomics (MCSG) III – Condition #4 (1.0 M Ammonium phosphate dibasic, 0.1 M imidazole/HCl) (A). Screening this original hit against the Hampton Additive Screen (Hampton Research) resulted in a much improved crystal form with Hampton Additive Screen Condition #52 (40% v/v pentaerythritol ethoxylate) (B).

These small, needle-like crystals were then screened against several additive screens, including the Hampton Additive Screen (Hampton Research), Hampton Detergent Screen (Hampton Research), Opti-Salts Screen (QIAGEN), and Silver Bullet Screen (Hampton Research). The largest improvement was seen in the Hampton Additive Screen from condition #52 (40% v/v pentaerythritol ethoxylate). Using MCSG III condition #4 as the initial condition and adding Hampton Additive Screen condition #52 to a final concentration of 10% v/v, produced very large, well-defined crystals. Although these conditions allowed for the successful, consistent reproduction of large, well-formed crystals, the crystals did not diffract sufficiently for full data collection. Despite the lack of high quality diffraction, enough diffraction data was collected to obtain preliminary structural information, including unit cell characterization (Table 2).

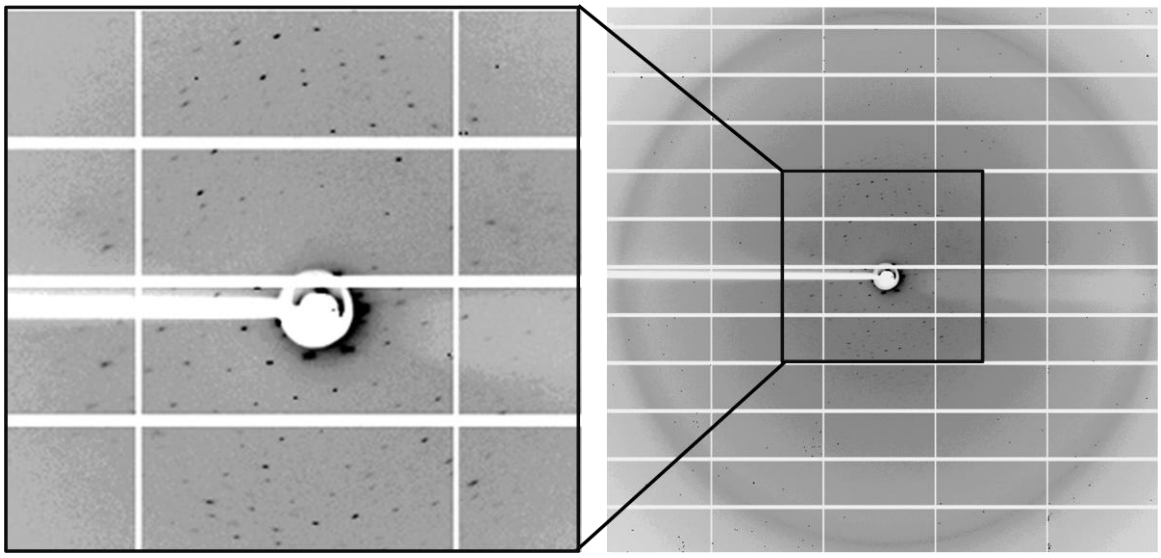

Figure 3.10 – X-ray diffraction data from a crystal of full-length PprA from *D. geothermalis*. Enlarged image of X-ray diffraction pattern (left) shows Bragg

spots visible to a resolution of 8Å. Crystals were exposed for 2 seconds in 1° increments at a wavelength of 0.9791 Å. Data was collected at the National Synchrotron Light Source (NSLS) on X25 beamline, at Brookhaven National Laboratory. Data was processed and scaled with HKL2000.

Table 2:	Unit cell characterization of PprA (*D. geothermalis*)
Bravais lattice	Primitive rhombohedral
Space Group	R3
Unit Cell Dimensions (Å)	132.15 x 132.15 x 598.12
Unit Cell Angles (°)	$\alpha = 90$ $\beta = 90$ $\gamma = 120$
Wavelength (Å)	0.9791
Resolution (Å)	50.00 - 8.00

Unit cell characterization included identification of the Bravais lattice, space group, and unit cell parameters (dimensions). The very large unit cell of the *D. geothermalis* PprA crystal is suggestive of a large assembly in the crystal lattice, perhaps reflecting the filament assembly observed by TEM. These data are consistent with the viscosity of the cell lysate when purifying this protein, as well as its elution at a high molecular weight (MW) in gel filtration studies. In the case of XLF, which also forms extended filaments, a similar large unit cell axis was also observed (~750 Å) (Andres and Junop, 2011), providing supporting evidence that these two proteins may be structurally and/or functionally related.

3.7 CRYSTALLIZATION OF PPRA FROM *D. RADIODURANS*

Of the various protein constructs of PprA from *D. radiodurans,* including full-length, as well as six N- and C-terminal truncations expressed with different fusion tags, the $PprA_{9-284}$ truncation from *D. radiodurans* represented both the most soluble, and highest yielding construct. As such, all crystallography trials of PprA from *D.* radiodurans were conducted using the $PprA_{9-284}$ protein.

A significant effort was put forth to crystallize $PprA_{9-284}$ from *D. radiodurans*. Table 3 outlines crystal hits of *D. radiodurans* $PprA_{9-284}$ generated from several initial broad screens, as well as further additive screens (Appendix A). Although much smaller in size than the full-length *D. geothermalis* PprA crystals, these diffracted to ~10 Å at the NSLS X25 beamline at Brookhaven National Laboratory (data not shown).

A systematic approach was taken in an attempt to optimize the weakly diffracting crystals from *D. radiodurans*. This included varying components of initial crystallization conditions, adjusting pH, temperature, drop ratio of protein/crystallization condition, streak seeding, varying ammonium sulfate concentration in well reservoirs, and including nucleating agents such as Naomi's Nucleants (Molecular Dimensions). Although various optimization approaches failed to produce a significantly better diffracting crystal, efforts thus far suggest that a search for an appropriate detergent may be the best next step to improving PprA crystal quality.

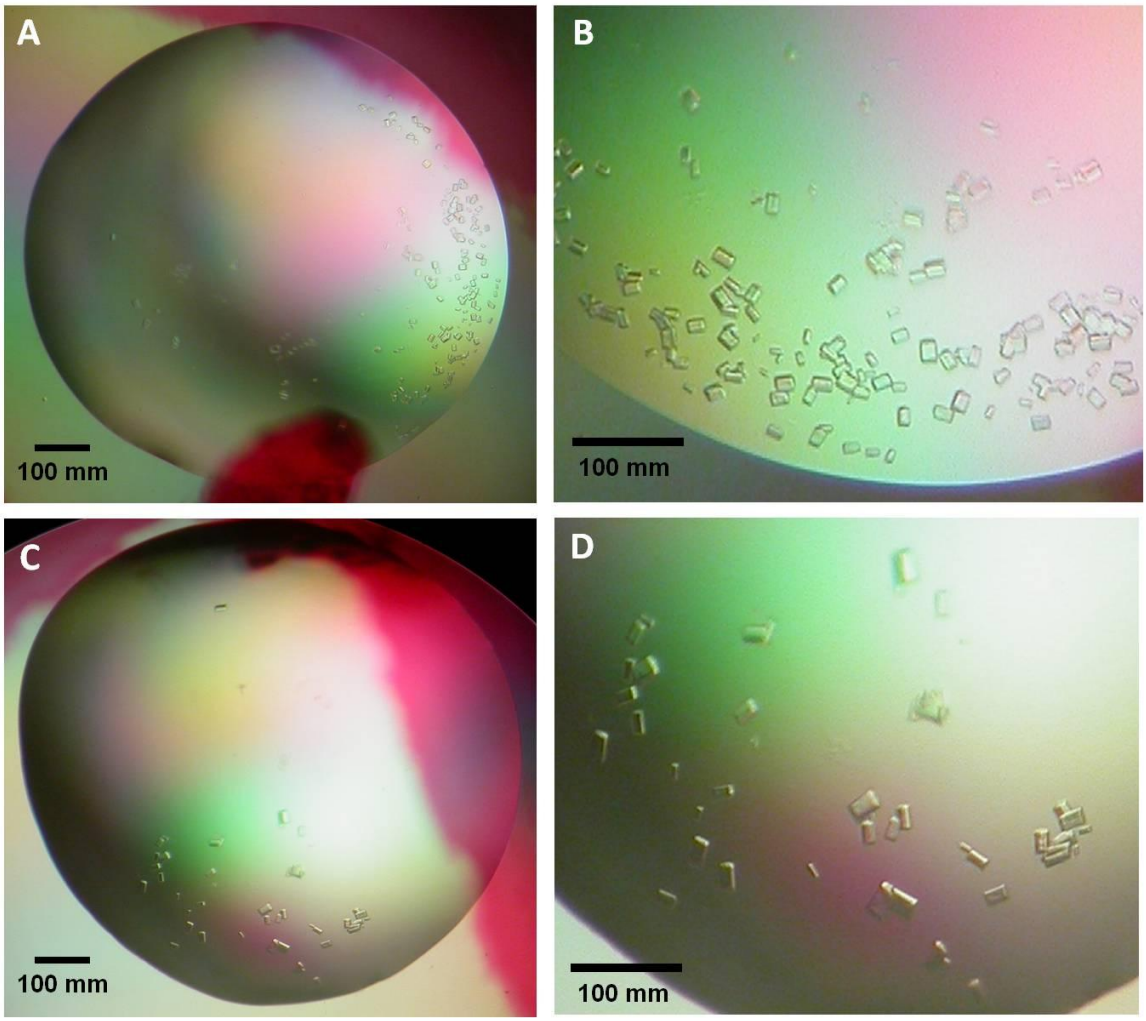

Figure 3.11 – Initial crystallization of $PprA_{9-284}$ from *D. radiodurans.* (A-B) MCSG II Condition #26 (0.64M malonic acid, 0.088M ammonium citrate tribasic, 0.042M succinic acid, 0.105M C2DL-malic acid, 0.14M sodium acetate, 0.175M sodium formate, 0.056M ammonium tartrate dibasic, final pH 7.0 with QIAGEN Opti-Salts Screen Condition #79 (0.1M sodium acetate pH 4.6, 3.5M sodium nitrate). (C-D) MCSG II Condition #26 with QIAGEN Opti-Salts Screen Condition #80 (3.5M sodium nitrate).

3.8 CRYSTALLIZATION OF *DEINOCOCCUS* PPRA HOMOLOGS

To increase the likelihood of solving the 3D crystal structure of PprA, homologs of PprA from *Deinococcus* species other than *D. geothermalis* and *D. radiodurans* were more recently explored. These included homologs of PprA from *D. peraridilitoris*, *D. maricopensis*, *D. gobiensis* and *D. deserti*.

Initial attempts to crystallize PprA from *D. peraridilitoris* were met with limited success. Full-length PprA from *D. peraridilitoris* was screened against the entire MCSG core suite I, II, III and IV (Microlytic), at both 20°C and 4°C. To date, no crystallization conditions have produced an initial crystal hit. PprA of other species, *D. maricopensis*, *D. gobiensis*, and *D. deserti* were not screened due to a lack of time.

3.9 *IN VIVO* COMPLEMENTATION STUDIES

To further explore the biological role that PprA may play in extreme DNA DSB repair, *in vivo* complementation studies were performed. These experiments were conducted to test for recovery following DNA damage induced by UV radiation. Full-length wild type PprA from *D. radiodurans*, as well as six N- and C-terminal truncations were cloned into a *Deinococcus* complementation shuttle vector. A survival assay was performed to test for the ability of the complemented strains of *D. radiodurans* to recover from severe DNA damage induced by UV radiation.

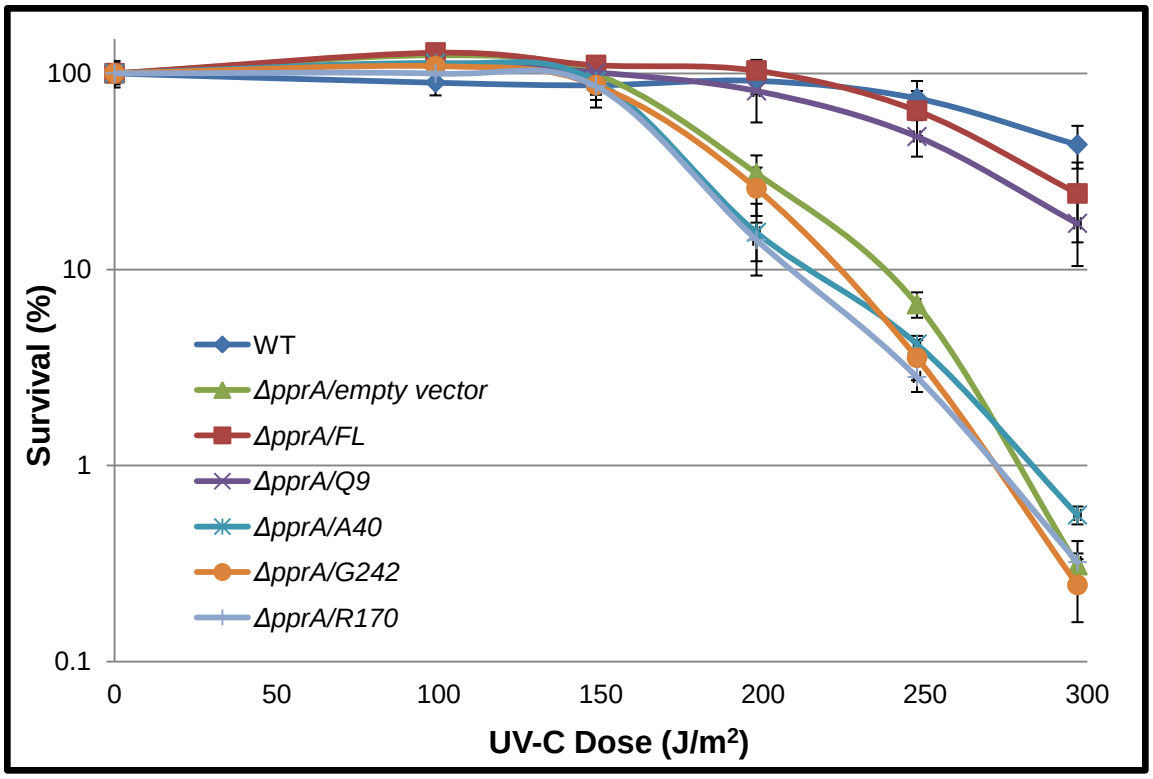

Figure 3.12 – Survival curve of TNK105, Δ*pprA D. radiodurans* cells complemented with various versions of *pprA*. Wild type *D. radiodurans* R1 strain is displayed in blue.

From the *in vivo* complementation assay results, full-length wild type *pprA* was able to reconstitute the UV resistance in *D. radiodurans* cells, at comparable levels to the native WT strain. Similarly, $PprA_{9\text{-}284}$ expressed in TNK105 was also able to recover from UV-induced damage at similar levels to those of the native WT strain.

Unlike Δ*pprA*/FL and Δ*pprA*/Q9, which were readily able to recover from UV-induced DNA damage similar to WT, the remaining PprA truncations tested

($PprA_{40-284}$, $PprA_{1-242}$ and $PprA_{1-170}$) were unable to recover from UV-induced damage to any greater extent than the *pprA* knockout strain, TNK105.

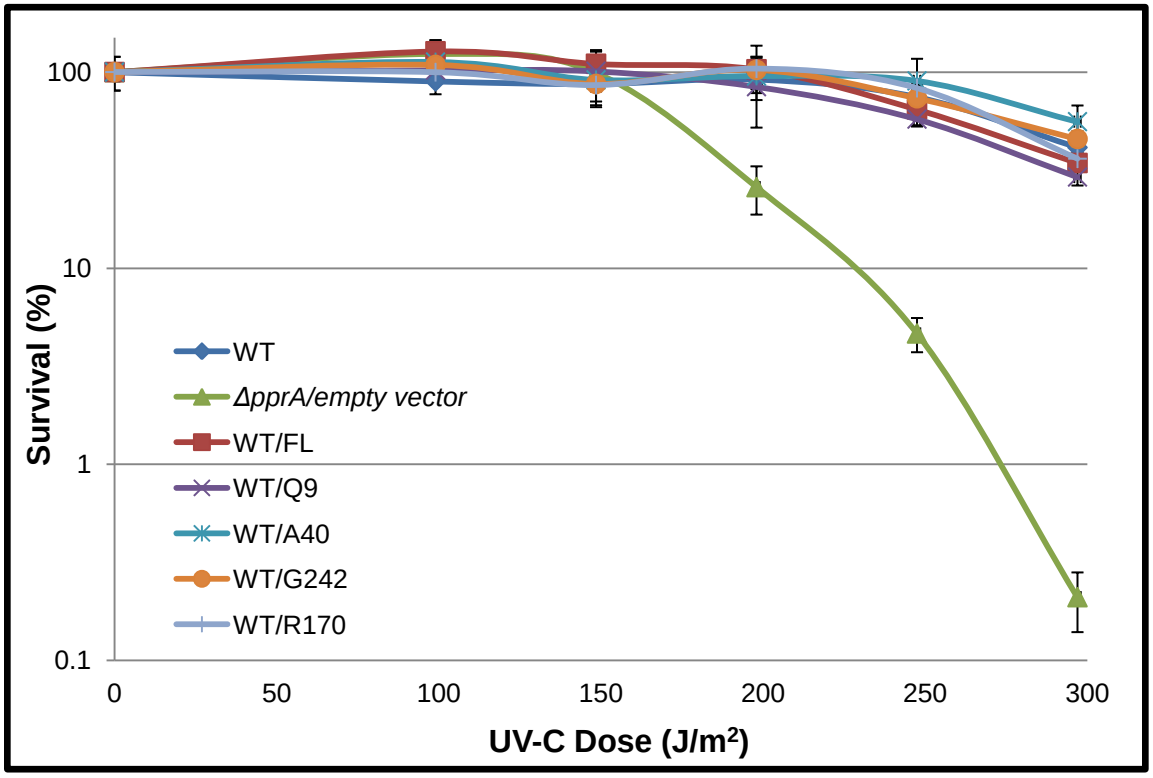

Figure 3.13 – Survival curve of wild type *D. radiodurans* R1 cells transformed with *Deinococcus* shuttle vector containing various deletions of *pprA*. This analysis was performed to test for potential dominant-negative behaviour.

As expected, full-length PprA complemented into the knockout strain, TNK105, was able to recover WT levels of UV-C resistance. PprA truncations, with the exception of $PprA_{9-284}$, produced a UV-C sensitive profile for TNK105/c, indicating these mutants had lost ability to function in DNA repair. Interestingly, $PprA_{9-284}$ was the only truncation that was able to reconstitute UV resistance to

levels similar to those of the full-length complement, and the WT *D. radiodurans* R1 strain (Figure 3.13).

To test for possible dominant negative effects, experiments were performed expressing PprA truncations in a wild type R1 strain (Figure 3.14). A UV survival assay was performed as described in section *2.8.2*. Results showed that the transformed cells behaved similar to the wild type R1 strain, and failed to produce a dominant negative effect, further indicating that these mutants most likely failed to form filaments perhaps as a result of misfolding. Follow-up studies with *in vitro* experiments to test for DNA binding and filament formation were unsuccessful.

CHAPTER 4 – DISCUSSION

CHAPTER 4. DISCUSSION

4.1 GENERAL DISCUSSION

The *Deinococcaceae*, are characterized by an extraordinary resistance to an array of DNA damaging agents. These bacteria can mend over 200 DSBs that result from exposure to IR, UV radiation, desiccation, or chemical agents, whereas only a few DSBs are lethal in nearly all other living organisms. This feat has been attributed to the combination of a number of protective mechanisms including protection of the proteome by ROS-scavenging complexes, as well as an efficient DSB repair pathway consisting of DNA repair proteins uniquely found in *Deinococcus* spp.

Of the five genes that are highly expressed in *D. radiodurans* in response to IR and desiccation, *pprA* was among the three (along with *ddrA* and *ddrB*) that were found to affect radiation resistance upon their deletion.

BLAST search results have suggested that PprA has no similarity to any known proteins in organisms outside of the *Deinococcus* genus. Since PprA is unique to *Deinococcus* spp., it stands to reason that the lack of a known homolog suggests the function of the protein is in DNA repair. The overarching goal of this project was to understand how PprA is involved in DNA damage repair in *Deinococcus* spp..

4.2 PURIFICATION OF PPRA

4.2.1 Purification of PprA from D. geothermalis

Full-length PprA from *D. geothermalis* expressed very well in *E. coli* BL21(DE3) and could be purified. However, the final protein yields from 1 L of *E. coli* cells expressing PprA from *D. geothermalis* were very low, typically ranging from 0.05-0.15 μg purified protein. These very poor yields made subsequent characterization challenging.

4.2.2 Purification of PprA from D. radiodurans

Initial attempts to purify PprA from *D. radiodurans* resulted in limited success. Although the full-length PprA from *D. radiodurans* expressed very well in *E. coli* BL21(DE3) cells, the protein had a high propensity for aggregation and precipitation during the purification process. To combat these difficulties, multiple expression constructs of PprA from *D. radiodurans* were cloned. These constructs included various fusion tags (His_6, MBP, GST and NusA) fused to the PprA protein. Although the inclusion of a fusion tag improved solubility, the protein continued to precipitate during the purification process, preventing the successful purification of the full-length protein.

Interestingly, one of the 6 truncations described in section *2.1.3*, $PprA_{9\text{-}284}$, was highly soluble in the absence of any protein fusion tags, and remained in solution throughout the purification process. The purification of $PprA_{9\text{-}284}$ resulted

in very clean (>95% purity), homogenous protein. Typical final yields ranged from 5-10 mg PprA per 2 L of induced *E. coli* cell culture. As a result of the yield and purity of this particular truncation of PprA, the majority of the work described in this thesis was performed using this protein.

4.2.3 Purification of PprA from D. peraridilitoris

Full-length PprA from *D. peraridilitoris* was readily purified from *E. coli* BL21(DE3) cells, when expressed with an MBP tag fused to the N-terminus of the protein. Following purification on a Ni-IMAC column and digestion with TEV protease, PprA from *D. peraridilitoris* was subsequently purified using size exclusion chromatography. Exploiting the unusually large size of PprA in solution, PprA was found to elute cleanly in the void volume from an S200 gel filtration column, resulting in a high yielding (2-4 mg), clean protein (>95% purity). It is notable that PprA from the other *Deinococcus* species also eluted in the void volume from an S200 gel filtration column, suggesting an unusually large oligomeric assembly in solution. These observations led to the use of EM as a technique to explore PprA behaviour in solution.

4.3 DNA BINDING OF PPRA

Deletion of the *pprA* gene from *D. radiodurans* renders the organism very sensitive to IR. PprA is therefore essential to recovery following severe DNA damage in *Deinococcus* spp., and must play an integral role in the DSB repair pathway. As it has been identified as a key player in the DSB repair pathway, it

stands to reason that PprA at some point forms an interaction with DNA. To further investigate this, the DNA binding of PprA was studied through EMSA experiments.

4.3.1 PprA binds dsDNA independent of sequence

Given that DSBs can occur anywhere in the genome, and *Deinococcus* chromosomes undergo random fragmentation upon exposure to extreme doses of γ-radiation, it would seem reasonable that PprA would bind DNA independently of sequence. The lack of sequence-specificity was confirmed for PprA by testing DNA binding ability to a DNA ladder, made up of fragments of various sequence and size.

Consistent with other proteins involved in DSB repair, the DNA binding activity of PprA was independent of DNA sequence. This suggests that DNA binding of PprA is primarily mediated by electrostatic interactions between positively charged residues in PprA and negatively charged phosphate residues in the DNA backbone.

While proteins involved in DNA repair frequently lack sequence-specific DNA binding preference, they often exhibit varied affinities for different DNA structures. Human XRCC4, for instance, binds DNA with no sequence-specificity, but has a preference for dsDNA containing either a nick or a DSB (Modesti *et al*., 1999). This feature may serve as an advantage allowing DNA repair proteins to quickly recognize a specific type of damage for efficient repair.

In fact, preferential DNA binding of other NHEJ proteins, such as Ku 70/80, to certain forms of DNA have been demonstrated (Blier *et al*., 1993). In contrast, XLF has been reported to have an equal affinity for linear and closed circular plasmid DNA (Hentges *et al*., 2006).

4.3.2 PprA has structure-specific binding to dsDNA with a free end

To determine whether PprA exhibits DNA structure-specific binding activity, EMSAs were carried out with linear, nicked and supercoiled DNA. Products from these reactions were resolved by agarose gel electrophoresis. The results from the EMSA experiments revealed that PprA displays not only a preference for linear dsDNA, but that it actually requires linear DNA in order to bind. PprA was unable to bind to nicked or supercoiled plasmid DNA.

4.3.3 PprA displays a binding preference for long linear dsDNA

Subsequent characterization revealed that PprA displays a higher binding affinity for longer linear dsDNA substrates, versus shorter linear dsDNA substrates. This result suggests the involvement of PprA in the final stages of extreme DSB repair, as long dsDNA fragments are reassembled back into large circular chromosomes. The mechanistic basis for this unusual preference for long dsDNA substrates remains unclear. It is possible that the preference for longer DNA fragments might promote more stable DNA-protein interactions due to a yet undiscovered structural feature of PprA. Alternatively, the preference toward long DNA substrates may be linked to the idea that the DNA repair

complex encompasses a large section of DNA. In mammalian DSB repair the repair complex spans thousands of base pairs. Human XRCC4 demonstrates an unusual requirement for large DNA substrates (~300 bp) in order to form stable protein-DNA complexes (Modesti *et al*., 1999).

4.3.4 Parallels between PprA and human repair factor Ku 70/80

In addition to binding exclusively to dsDNA, PprA was previously shown to stimulate the NAD- and ATP-dependent DNA ligase activity of T4 DNA ligase (Narumi *et al*., 2004). These observations have led to the suggestion that PprA may function in a manner similar to the Ku 70/80 complex in the NHEJ pathway.

The initial step in the NHEJ pathway involves the recognition of a DSB by the Ku 70/80 heterodimer. Ku binds to DNA ends with a high affinity (Blier *et al*., 1993), limiting the amount of nucleolytic degradation that would otherwise lead to the loss of important genetic information. The structure of Ku 70/80 reveals a ring-like assembly, allowing DNA to move through a porous opening in the middle of the ring. Furthermore, the interior of the Ku 70/80 cavity is abundant in positively charged amino acid residues, further stabilizing Ku-DNA interactions. Ku 70/80 plays a central role in the NHEJ DSB repair pathway, acting initially as a DSB recognition factor, and then later as a scaffold protein for downstream repair factors that are recruited to the site of DSB damage. Along with DNA PKcs, Ku 70/80 forms a complex (Dvir *et al*., 1992) which aligns and bridges DNA ends for downstream repair (Spagnolo *et al*., 2006). PprA may be involved

in a similar interaction with an unknown binding partner, and align and bridge DNA, and protect the DNA from degradation in a comparable fashion.

The discovery that PprA has DNA-end binding activity, binding only to linear dsDNA, and not to nicked, or closed circular dsDNA supports a Ku-like behaviour. Additionally, the discovery that PprA stimulates the DNA end-joining reaction catalyzed by ATP- and NAD-dependent DNA ligase supports the proposed involvement of PprA in the final reassembly stages of DSB repair, in the reconstitution of large circular chromosomes, possibly by an NHEJ-like mechanism. However, the NHEJ mechanism is prone to error, which is inconsistent with the apparent error-free repair that is reported for *Deinococcus* spp.. Nevertheless, it seems reasonable to think that *Deinococcus* spp. might utilize an adapted NHEJ-like repair mechanism.

Given these hypotheses, crystallographic studies were carried out to determine if there is structural similarity between PprA and Ku 70/80. To this extent, a DNA substrate that was used in the structural determination of the Ku70/80 heterodimer is currently being used in crystallography trials in an effort to crystallize PprA bound to a DNA substrate which would stabilize the proposed ring-like structure onto DNA.

4.4 PPRA FILAMENT FORMATION

4.4.1 Filament formation is conserved between three Deinococcus species

Purified PprA from *D. geothermalis, D. radiodurans*, and *D. peraridilitoris* formed long fibrous filament networks *in vitro.* In comparing the morphology of the three different proteins, filaments from all three species looked different. The filaments from *D. radiodurans* $PprA_{9-284}$ for example, displayed a very regular striated pattern across the filament. The striations were observed to form highly repetitious alternating light/dark regions. The filaments formed by *D. peraridilitoris* PprA formed a similar striated pattern as in *D. radiodurans*. These striations, however, ran lengthwise along the filament. The difference in morphology is likely a result of difference in filament assembly from individual PprA monomers.

A DNA-binding mutant of *D. radiodurans*, $PprA_{9-284}$ G149E, also formed filaments, which showed no visible difference compared to filaments formed with wild type $PprA_{9-284}$. Based on these results, filament formation is likely not dependent on DNA binding.

4.4.2 Filament formation of PprA is reminiscent of human XRCC4/XLF

The observation that filament formation is conserved between three *Deinococcus* species strongly suggests biological significance. Whether these filaments are essential to DNA repair remains to be determined. Supporting the hypothesis that PprA filament formation may play an important biological role in DSB repair is the recent discovery that human XRCC4/XLF forms a filament that bridges DNA molecules. During DSB repair, DNA ends must be maintained in

close proximity throughout the assembly process. In mammalian cells, this is facilitated though a higher-order nucleoprotein complex composed of XRCC4 and XLF, which form an extended filament. This XRCC4/XLF filament binds DNA, but also bridges DNA ends (Andres *et al*., 2012).

4.4.3 Other filament forming proteins involved in DNA repair

Although a comparison has been made between PprA and XRCC4/XLF based on the formation of multifilament bundles observed *in vitro*, other proteins involved in DNA repair have also been reported to form filaments. Rad51, for example, forms filaments during DSB repair via HR (Chen *et al*., 2007; Conway *et al*., 2004). Additionally, RecA binds to ssDNA and forms a nucleoprotein filament. The RecA-ssDNA filament searches for sequence similarity along dsDNA, eventually initiating strand exchange in an HR repair manner.

It has been suggested that PprA is epistatic to RecA, as evidenced by radiation survival (Tanaka *et al*., 2004) and repair kinetics (Devigne *et al*., 2013) of a Δ*recA*/Δ*pprA* double deletion mutant. A *pprA recA* double mutant is as sensitive to IR as the *recA* mutant (Tanaka *et al*., 2004). It would therefore appear that RecA and PprA function in the same pathway. Thus, the recurring theme of protein filaments involved in DSB repair and DNA maintenance, suggests that protein filaments may be a specialized form of protein structure more widely involved in protecting genome integrity than previously realized. The observation of PprA filaments, provides the first clue of a potentially robust

mechanism to mediate higher-order nucleoprotein complex regulation and sorting of damaged DNA during extreme repair situations in *Deinococcus* spp..

4.5 A SEARCH FOR A FILAMENT DISRUPTING MUTANT

The observation that PprA forms large multimeric filaments in solution was very reminiscent of XRCC4/XLF DNA bridging factors that are involved in NHEJ DSB repair. In NHEJ, DNA Ligase IV, seals two broken DNA ends. In order to facilitate this reaction, XRCC4 and XLF first bridge the two broken DNA fragments together, forming a nucleoprotein filament bundle. This process led us to wonder whether PprA could be involved in an NHEJ-like repair mechanism in *Deinococcus* spp.. From what is currently known in the literature, there are no known XRCC4 or XLF homologs in any bacteria.

Despite obvious sequence similarity to any proteins outside of the *Deinococcus* genus, it remains possible that PprA may represent a *Deinococcus* homolog of human XLF. Similar to XLF, PprA interacts with DNA, and displays a preference for unusually long DNA.

4.5.1 Generation of PprA point mutants to disrupt filament formation based on XRCC4/XLF structure

Looking at interacting amino acid residues between human XRCC4 and XLF, there is an interaction between the α2 and α3 patch of the proteins. Based on the structure of these two proteins, the amino acid residues involved in

interaction are K99, K65, D58, and F106 in XRCC4, and L115, R64 and E111 in XLF. Using these amino acid residues, and the comparison of secondary structure prediction of PprA, amino acids were selected that might correspond to exposed hydrophobic residues used by XRCC4/XLF to establish filament formation. Three amino acid residues were identified from the secondary structure prediction models of PprA from *D. radiodurans*. The amino acid sequence between the seventh and eighth predicted alpha helices of PprA from strongly resembled the amino acid sequence found between the α2 and α3 patch of the XRCC4/XLF proteins. With this information, site-directed mutants targeting amino acids L164, F165 and V166 were created. Each residue was changed to an aspartic acid residue (D).

The observation that $PprA_{9\text{-}284}$ L164D, F165D, and V166D all form filaments indistinguishable from WT indicates that these particular mutations do not alter filament formation. Despite this result, it remains a possibility that PprA and XRCC4/XLF are either structural or functional homologs.

4.5.2 Testing PprA for the ability to complement XRCC4/XLF in eukaryotic cells

Nej1, in *S. cerevisiae*, is very different in sequence from XLF (~12% sequence identity). Despite this, it has been shown that these proteins are structural homologs (Callebaut *et al*., 2006). Nej1 interacts with Lif1, which was identified as an XRCC4 homolog in yeast (Herrmann *et al*., 1998). Although the sequences of Nej1 and Lif1 are very different from XLF and XRCC4, these

proteins are functional homologs. Using the Nej1 protein as an example, it remains a possibility that PprA, despite very low sequence similarity with XLF, may still be a functional homolog of this DNA repair protein.

In order to test this idea, PprA from *D. radiodurans* was complemented into ΔXLF and ΔXRCC4 human cells, for survival studies. The objective of these experiments was to see if PprA was functionally redundant to XLF or XRCC4. In collaboration with Dr. Kathryn Meek at Michigan State University, 9 clones were made (with both NLS and V5 tags in Abelson cell lines), expressing high levels of PprA. The hypothesis was that XRCC4/XLF filaments and PprA filaments would promote DSB repair to similar levels. This did not seem to be the case. Whereas XLF complementation significantly restored DSB repair, the PprA complement was unable to restore DSB repair.

4.5.3 Testing PprA for DNA bridging activity

To further test whether PprA could act like XLF and XRCC4 in NHEJ-like repair in *Deinococcus* spp., PprA was tested in a DNA bridging assay (Mauro Modesti, CNRS, France). Under conditions that showed XRCC4 and XLF bridging DNA, PprA did not bridge DNA. Although this suggests that PprA does not function as a DNA bridging factor, the results indicate PprA does not bridge dsDNA under the specific conditions tested. It remains a possibility that under different bridging conditions, PprA may still possess the ability to bridge dsDNA, however these different conditions remain to be explored.

The speculation that PprA may function in an NHEJ-like DSB repair pathway by acting as a DNA bridging factor to align and link two DNA fragments is still in question. To clearly establish this or other links to known DNA repair factors, a structure of PprA will be needed.

4.6 MULTIPLE SEQUENCE ALIGNMENT AND SECONDARY STRUCTURE PREDICTION MODELS OF PPRA

The complete genomes of 6 of the 48 species of *Deinococcus* have been sequenced. A multiple sequence alignment of PprA from these 6 *Deinococcus* spp. can be found in Appendix D. The level of conservation is very high amongst all PprA homologs. Alignment of the N-terminus of PprA is consistently weaker, compared to the rest of the protein. The disorder profiles for PprA from these six homologs are found in Appendix C. Consistent with the multiple sequence alignments, the N-terminus of each protein is predicted to be highly disordered, according to the DISOPRED2 disorder prediction tool (PSIPRED). This region contains significant hydrophilic nature. Such regions do not typically form secondary structure. The highly variant and disordered N-terminal region of PprA could suggest why the N-terminal truncation, $PprA_{9-284}$, was well-behaved, compared to full-length versions of the protein. Furthermore, the remaining truncations were more challenging to work with possibly due to protein misfolding caused by a highly disordered N-terminus, or too large of a deletion. It appears,

based on these observations, that the N-terminus of PprA is important for proper protein folding.

4.7 CRYSTALLOGRAPHIC STUDIES

Structure determination by X-ray crystallography was one of the main approaches taken to gain insight into the molecular mechanism of PprA. A three dimensional, atomic resolution structure of PprA could reveal information regarding the possible structural similarity with XLF/XRCC4 or Ku 70/80. In addition, it could offer clues about the mechanisms by which this protein engages DNA and assembles into higher order filaments.

Utilizing an approach similar to one taken by a larger Structural Genomics Consortium (SGC), a systematic multi-construct approach was used to obtain soluble protein. Not every protein can be expressed in *E. coli* in soluble form. Proteins that fail to express in a soluble form may be toxic to the host or could reflect lack of proper modifications or an inability to fold in the bacterial system. It has been well reported that levels of expression and the degree of solubility of a recombinant protein expressed in *E. coli* can be greatly influenced by even slight variation in the amino acid sequence at the N- and C-terminus. In addition to systematic N- and C-terminal deletions, the addition of several different fusion tags to promote expression and solubility of the recombinant protein were used in the multi-construct approach, increasing the chances of obtaining soluble protein.

In turn, the chances of obtaining well-diffracting crystals were further increased by this approach.

The N- and C-terminal truncations of PprA from *D. radiodurans* were designed not only to potentially identify a region of the PprA protein responsible for mediating filament formation, but also with the idea that one or more might be useful in structure determination trials. Large heterogeneous filaments resist ordered crystal packing. A PprA truncation devoid of this formation might therefore increase the chances of determining the crystal structure of at least part of PprA.

4.7.1 Crystallographic trials for PprA from D. geothermalis

A significant effort was made to crystallize apo-PprA, as well as PprA bound to DNA. Full-length PprA from *D. geothermalis* was the first target protein subjected to crystallization trials. The initial trials with broad crystallization screens yielded several conditions that produced “showers” of nucleation, with several hundreds of very small crystals per drop. These initial crystal ‘hits’ were small, with long, sharp needle-like appearance. Subsequent crystal optimization with additive screens yielded significantly larger crystals with well defined edges. Unfortunately these crystals did not diffract sufficiently for full data collection. Despite the lack of high quality diffraction, enough data was collected to obtain preliminary structural information, including unit cell characterization (Table 2.).

A very interesting observation was the unusually long unit cell axis (~600 Å) in one dimension of the crystal. This abnormally long unit cell axis was reminiscent of a unit cell axis of the XLF/XRCC4 protein crystal (~750 Å). A very long unit cell axis typically reflects abnormal crystal packing, resulting from large oligomeric structures such as filaments. The resulting crystal packing of such filaments may also weaken crystal contacts leading to poor quality diffraction data.

4.7.2 Crystallographic trials for PprA from D. radiodurans

The greatest amount of time and effort was invested in crystallizing $PprA_{9-284}$ from *D. radiodurans.* Although not the full-length version of the protein, structural information of even a fragment of a protein can reveal valuable information. Screening against several broad screens, and subsequent additive screens yielded several conditions that produced crystals (see: Table 3; Appendix A). Although various optimizing approaches failed to significantly improve crystal quality, a pattern of certain chemical components common to multiple conditions that generated crystals was derived. This redundancy suggested that certain chemical components may be critical to crystal formation. These chemicals included ammonium phosphate, imidazole:HCl, PEG 3350, potassium citrate, and various detergents.

Over 10,000 unique crystallization conditions were screened for diffraction quality crystals. Since various optimization approaches failed to produce better

diffracting crystals, crystallization trials for PprA from additional species will be performed in an effort to generate a high quality diffracting crystal. These include PprA from *D. gobiensis*, *D. maricopensis*, *D. deserti*, and *D. peraridilitoris.*

Although a crystal structure of apo-PprA would be very informative, arguably more valuable would be a crystal structure of PprA bound to DNA. In order to better dictate future structural studies, the choice of a well-defined DNA substrate is critical to obtain a crystal structure of protein bound to DNA. Ongoing efforts in the lab will need to focus on identifying a proper DNA substrate to use in future crystallographic experiments.

4.8 *IN VIVO* CHARACTERIZATION OF PPRA

In vivo characterization of PprA through complementation experiments monitoring recovery following UV-induced DNA damage showed that various truncations of PprA did not produce a dominant negative effect on damage recovery. Although the deletions displayed no ability to restore DSB repair, it is not clear if this was a specific effect attributed to loss of filament formation, or protein misfolding. An *in vitro* assay to further explore function of these deletions is needed to distinguish between these possibilities.

4.9 PHOSPHORYLATION OF PPRA

Rajpurohit and Misra (2013) recently reported that PprA residues threonine 72 (T72), serine 112 (S112) and threonine 144 (T144) are rapidly

phosphorylated in response to DNA damage. This phosphorylation was shown to be required for efficient DNA repair *in vivo* (Rajpurohit and Misra, 2013). Furthermore, phosphorylation of PprA increased its affinity for DNA 4-fold, and could enhance its supportive role in intermolecular ligation by T4 DNA ligase (Rajpurohit and Misra, 2013). These results suggest that phosphorylation of PprA plays an important role in radiation resistance of *D. radiodurans*.

Comparing the necessity for phosphorylation of PprA, to other DNA repair proteins, XRCC4 in humans is phosphorylated *in vivo* in a DNA-PK dependent manner (Modesti *et al*., 1999). Phosphorylated XRCC4 was able to stimulate end-joining by DNA Ligase IV (Modesti *et al*., 1999), in much the same way that PprA has been shown to stimulate end joining by T4 DNA Ligase (Narumi *et al*., 2004).

Phosphorylation of PprA may or may not be accompanied by a conformational change. The role of PprA phosphorylation in extreme DSB repair in *Deinococcus* spp. appears to be important, however additional experiments exploring the functional significance of PprA phosphorylation in end-joining are required to evaluate the mechanism of this regulation further. It would be very interesting to test the effects of pseudo phosphorylation mimics of PprA's known phosphorylation sites on its ability to form filaments.

CHAPTER 5 – CONCLUSIONS & FUTURE RESEARCH DIRECTIONS

CHAPTER 5. CONCLUSION AND FUTURE RESEARCH DIRECTIONS

Many important questions regarding PprA in the area of extreme DNA repair in *Deinococcus* spp. remain unanswered. Does PprA recruit other proteins to the site of DNA damage? If so, what are they and are the functions known? Is there structural similarity to other DNA repair proteins, such as Ku 70/80, that would suggest an end-alignment function, degradation protection function, or direct interaction with DNA Ligase? Is there structural or functional similarity to human XRCC4/XLF, which would suggest a DNA bridging function? A complete structural characterization of PprA, both on its own, and in complex with DNA, would undoubtedly yield the most significant functional and mechanistic insight to these questions.

Additional analysis of the DNA binding behaviour of PprA should reveal whether its binding is cooperative. Cooperative binding would suggest that PprA forms higher order complexes with varying DNA binding affinities, or that PprA contains multiple DNA binding sites where the binding of DNA to the first site improves binding at the second site. Such cooperative DNA binding behaviour of PprA would be consistent with a protein that may function to bridge two DNA molecules during repair through formation of filaments such as those observed for XRCC4/XLF.

Atomic force microscopy (AFM) is one of two techniques (along with EM), that allows for direct visualization of DNA. The interaction between PprA and

DNA, as well as other potential partners, such as *Deinococcal* Ligase A, *Deinococcal* Ligase B, or DdrB can be visualized using AFM. To determine whether a direct interaction with DNA ligase exists, both DNA Ligase A, and DNA Ligase B, from *D. radiodurans*, have recently been obtained in order to carry out these interaction studies. Preliminary data from a pull-down experiment using His_6-DdrB and lysate from γ-irradiated *D. radiodurans* cells suggests that PprA forms a stable interaction with DdrB (data not shown). While DdrB has been shown to be involved in annealing of ssDNA in the SSA pathway, it is possible that DdrB also participates in other aspects of the DSB repair mechanism in *Deinococcus* spp., forming an interaction with PprA. The recent discovery that PprA and DdrB form a stable interaction *in vitro* is an important finding that requires further investigation.

Finally, with respect to the filaments formed by three different *Deinococcus* spp., we still do not know if these filaments are important for PprA function in DNA repair and radiation resistance. Further work needs to be done to determine whether or not these filaments are important biologically. In order to properly answer these questions, there remains the need to identify a mutant that disrupts filament formation, followed by testing the effect on repair ability *in vivo*.

Characterizing the DNA binding ability and filament formation of PprA is essential to clarify its proposed function in bridging and aligning of DNA fragments in *Deinococcus* DSB repair following extreme damage.

REFERENCES

Aebi, U., and Pollard, T.D. (1987) A glow discharge unit to render electron microscope grids and other surfaces hydrophilic. *Journal of Electron Microscopy Technique*. **7**: 29-33.

Anderson, A.W., Nordan, H.C., Cain, R.F., Parrish, G., and Duggan, D. (1956) Studies on a radio-resistant *micrococcus*. I. Isolation, morphology, cultural characteristics, and resistance to gamma radiation. *Food Technology*. **10**: 575-577.

Anderson, D.G. and Kowalczykowski, S.C. (1997) The recombination hot spot chi is a regulatory element that switches the polarity RecBCD enzyme. *Genes and Development*. **11**: 571-581.

Andres, S.N., and Junop, M.S. (2011) Crystallization and preliminary X-ray diffraction analysis of the human XRCC4-XLF complex. *Acta Crystallographica. Section F, Structural Biology and Crystallization Communications.* **67**:: 1399-1402.

Andres, S.N., Vergnes, A., Ristic, D., Wyman, C., Modesti, M., and Junop, M. (2012) A human XRCC4-XLF complex bridges DNA. *Nucleic Acids Research*. **4**: 1868-1878.

Anjem, A., Varghese, S., and Imlay, J.A. (2009) Manganese import is a key element of the OxyR response to hydrogen peroxide in *Escherichia coli*. *Molecular Microbiology*. **72**: 844-858.

Archibald, F.S., and Fridovich, I. (1982) The scavenging of superoxide radical by manganous complexes: in vitro. *Archives of Biochemistry and Biophysics*. **214**: 452-463.

Arrage, A.A., Phelps, T.J., Benoit, R.E., Palumbo, A.V., and White, D.C. (1993) Bacterial sensitivity to UV light as a model for ionizing radiation resistance. *Journal of Microbiological Methods.* **18**: 127-136.

Appukuttan, D., Rao, A.S., and Apte, S.K. (2009) Engineering of *Deinococcus radiodurans* R1 for bioprecipitation of uranium from dilute nuclear waste. *Applied*

Environmental Microbiology. **72**: 7873-7878

Battista, J.R. (1997) Against all odds: the survival strategies of *Deinococcus radiodurans*. *Annual Review of Microbiology*. **51**: 203-224.

Barnese, K., Gralla, E.B., Cabelli, D.E., and Valentine, J.S. (2008) Manganous phosphate acts as a superoxide dismutase. *Journal of the American Chemical Society*. **130**: 4604-4606.

Bauermeister, A., Bentchikou, E., Moeller, R., and Rettberg, P. (2009) Roles of PprA, IrrE, and RecA in the resistance of *Deinococcus radiodurans* to germicidal and environmentally relevant UV radiation. *Archives of Microbiology*. **191**: 913-918.

Bentchikou, D.A., Servant, P., Coste, G., and Sommer, S. (2010) A major role of the RecFOR pathway in DNA double-strand-break repair through ESDSA in *Deinococcus radiodurans*. *PLoS Genetics*. **6**: e1000774.

Berlett, B.S., Chock, P.B., Yim, M.B., and Stadtman, E.R. (1990) Manganese (II) catalyzes the bicarbonate-dependent oxidation of amino acids by hydrogen peroxide and the amino acid-facilitated dismutation of hydrogen peroxide. *Proceedings of the National Academy of Sciences*. **87**: 389-393.

Bernstein, D.A., Eggington, J.M., Killoran, M.P., Misic, A.M., Cox, M.M., and Keck, J.L. (2004) Crystal structure of the *Deinococcus radiodurans* single-stranded DNA-binding protein suggests a mechanism for coping with DNA damage. *Proceedings of the National Academy of Sciences*. **101**: 8575-8580.

Bessman, M.J., Frick, D.N., and O'Handley, S.F. (1996) The MutT proteins or "Nudix" hydrolases, a family of versatile, widely distributed, "housecleaning" enzymes. *Journal of Biological Chemistry*. **271**: 25059-25062.

Blasius, M., Sommer, S., and Hübscher, U. (2008) *Deinococcus radiodurans*: what belongs to the survival kit? *Critical Reviews in Biochemistry and Molecular Biology*. **43**: 221-238.

Blier, P.R., Griffith, A.J., Craft, J., and Hardin, J.E. (1993) Binding of Ku protein to DNA – Measurement of affinity for ends and demonstration of binding to

nicks. *Journal of Biological Chemistry* **10**: 7594-7601.

Brim, H., Osborne, J.P., Kostandarithes, H.M., Fredrickson, J.K., Wackett, L.P., and Daly, M.J. (2006) *Deinococcus radiodurans* engineered for complete toluene degradation facilitates Cr(VI) reduction. *Microbiology*. **152**: 2469-2477.

Burrell, A.D., Feldschreiber, P., and Dean, C.J. (1971) DNA-membrane association and the repair of double breaks in x-irradiated *Micrococcus radiodurans*. *Biochimica et Biophysica Acta*. **247**: 38-53.

Callebaut, I., Maliverty, L., Fischer, A., Mornon, J.P., Revy, P., and de Villartay, J.P. (2006) Cernunnos interacts with the XRCC4 x DNA-ligase IV complex and is homologous to the yeast nonhomologous end-joining factor Nej1. *Journal of Biological Chemistry*. **281**: 13857-13860.

Carroll, J.D., Daly, M.J., and Minton, K.W. (1996) Expression of *recA* in *Deinococcus radiodurans*. *Journal of Bacteriology*. **178**: 130-135.

Chen, L.T., Ko, T.P., Chang, Y.C., Lin, K.A., Chang, C.S., Wang, A.H., and Wang, T.F. (2007) Crystal structure of the left-handed archael RadA helical filament: identification of a functional motif for controlling quaternary structures and enzymatic functions of RecA family proteins. *Nucleic Acids Research*. **35**: 1781-1801.

Chou, F.I., and Tan, S.T. (1990) Manganese(II) induces cell division and increases in superoxide dismutase and catalase activities in an aging *deinococcal* culture. *Journal of Bacteriology*. **172**: 2029-2035.

Conway, A.B., Lynch, T.W., Zhang, Y., Fortin, G.S., Fung, C.W., Symington, L.S. and Rice, P.A. (2004) Crystal structure of a Rad51 filament. *Nature Structural and Molecular Biology*. **11**: 791-796.

Copeland, A., Zeytun, A., Yassawong, M., Nolan, M., Lucas, S., Hammon, N., Deshpande, S., Cheng, J.F., Han, C., Tapia, R., Goodwin, L.A., Pitluck, S., Mavromatis, K., Liolios, K., Pagani, I., Ivanova, N., Mikhailova, N., Pati, A., Chen, A., Palaniappan, K., Land, M., Hauser, L., Jeffries, C.D., Brambilla, E.M., Rohde, M., Sikorski, J., Pukall, R., Göker, M., Detter, J.C., Woyke, T., Bristow, J., Eisen, J.A., Markowitz, V., Hugenholtz, P., Kyrpides, N.C., Klenk, H.P., and

Lapidus, A. (2012) Complete genome sequence of the orange-red pigmented, radioresistant *Deinococcus proteolyticus* type strain (MRP(T)). *Standards in Genomic Sciences*. **6**: 240-250.

Cox, M.M., and Battista, J.R. (2005) *Deinococcus radiodurans* – the consummate survivor. *Nature Reviews Microbiology*. **3**: 882-892.

Daly, M.J., and Minton, K.W. (1995) Interchromosomal recombination in the extremely radioresistant bacterium *Deinococcus radiodurans*. *Journal of Bacteriology*. **177**: 5495-5505

Daly, M.J., and Minton, K.W. (1996) An alternative pathway of recombination of chromosomal fragments precedes *recA*-dependent recombination in the radioresistant bacterium *Deinococcus radiodurans*. *Journal of Bacteriology*. **176**: 3508-3517.

Daly, M.J., Gaidamakova, E.K., Matrosova, V.Y., Vasilenko, A., Venkateswaran, A., Hess, M., Omelchenko, M.V., Kostandarithes, H.M., Makarova, K.S., Wackett, L.P., Fredrickson, J.K., and Ghosal, D. (2004) Accumulation of Mn(II) in *Deinococcus radiodurans* facilitates gamma-radiation resistance. *Science*. **306**: 1025-1028.

Daly, M.J., Gaidamakova, E.K., Matrosova, V.Y., Vasilenko, A., and Zhai, M. (2007) Protein oxidation implicated as the primary determinant of bacterial radioresistance. *PLoS Biology*

Daly, M.J., Gaidamakova, E.K., Matrosova, V.Y., Kiang, J.G., Fukumoto, R., Lee, D.Y., Wehr, N.B., Viteri, G.A., Berlett, B.S. and Levine, R.L. (2010) Small-molecule antioxidant proteome-shields in *Deinococcus radiodurans*. *PLoS ONE.* **5**: e12570.

de Groot, A., Dulermo, R., Ortet, P., Blanchard, L., Guérin, P., Fernandez, B., Vacherie, B., Dossat, C., Jolivet, E., Siguier, P., Chandler, M., Barakat, M., Dedieu, A., Barbe, V., Heulin, T., Sommer, S., Achouak, W., and Armengaud, J. (2009) Alliance of proteomics and genomics to unravel the specificities of Sahara bacterium *Deinococcus deserti*. *PLoS Genetics*. **5**: e1000434.

Devigne, A., Mersaoui, S., Bouthier de la Tour, C., Sommer, S., and Servant, P. (2013) The PprA protein is required for accurate cell division of gamma-irradiated *Deinococcus radiodurans* bacteria. *DNA Repair (Amst.)*. **12**: 265-272.

Dvir, A., Peterson, S.R., Knuth, M.W., Lu, H., and Dynam, W.S. (1992) Ku autoantigen is the regulatory component of a template-associated protein kinase that phosphorylates RNA polymerase II. *Proceedings of the National Academy of Sciences*. **24**: 11920-11924.

Eltsov, M., and Dubochet, J. (2005) Fine structure of the *Deinococcus radiodurans* nucleoid revealed by cryoelectron microscopy of vitreous sections. *Journal of Bacteriology*. **187**: 8047-8054.

Fredrickson, J.K., Li, S.M., Gaidamakova, E.K., Matrosova, V.Y., Zhai, M., Sulloway, H.M., Scholten, J.C., Brown, M.G., Balkwill, D.L., and Daly, M.J. (2008) Protein oxidation: key to bacterial desiccation resistance? *The ISME Journal*. **4**: 393-403.

Gerard, E., Jolivet, E., Prieur, D., and Forterre, P. (2001) DNA protection mechanisms are not involved in the radioresistance of the hyperthermophilic archaea *Pyrococcus abyssi* and *P. furiosus*. *Molecular Genetics and Genomics*. **266**: 72-78.

Hansen, M.T. (1978) Multiplicity of genome equivalents in the radiation-resistant bacterium Micrococcus radiodurans. *Journal of Bacteriology*. **134**: 71-75.

Harris, D.R., Tanaka, M., Saveliev, S.V., Jolivet, E., Earl, A.M., Cox, M.M., and Battista, J.R. (2004) Preserving genome integrity: the DdrA protein of *Deinococcus radiodurans* R1. *PLoS Biology*. **2**: e304.

Harsojo, Kitayama, S. and Matsuyama, A. (1981) Genome multiplicity and radiation resistance in *Micrococcus radiodurans*. *Journal of Biochemistry*. **90**: 877-880.

Hentges, P., Ahnesorg, P., Pitcher, R.S., Bruce, C.K., Kysela, B., Green, A.J., Bianchi, J., Wilson, T.E., Jackson, S.P. and Doherty, A.J. (2006) Evolutionary and functional conservation of the DNA non-homologous end-joining protein, XLF/Cernunnos. *Journal of Biological Chemistry*. **281**: 37517-37526.

Herrmann, G., Lindahl, T., and Schär, P. (1998) *Saccharomyces cerevisiae* LIF1: a function involved in DNA double-strand break repair related to mammalian XRCC4. *The EMBO Journal*. **17**: 4188-4198.

Hu, Y., Tian, B., Xu, G., Yin, L., Hua, X, Lin, J., and Hua, Y. (2010) Characteristics of nuclease activity of the SbcCD complex from *Deinococcus radiodurans*. *Journal of Biochemistry*. **147**: 307-315.

Hutchinson, F. (1985) Chemical changes induced in DNA by ionizing radiation. *Progress in Nucleic Acid Research and Molecular Biology*. **32**: 115-154.

Imlay, J.A. (2003) Pathways of oxidative damage. *Annual Review of Microbiology*. **57**: 395-418.

Ito, H (1977) Isolation of *Micrococcus radiodurans* occurring in radurized sawdust culture media of mushroom. *Agricultural and Biological Chemistry*. **41**: 35-41.

Jolivet, E., Lecointe, F., Coste, G., Satoh, K., Narumi, I, Bailone, A., and Sommer, S. (2006) Limited concentration of RecA delays DNA double-strand break repair in *Deinococcus radiodurans* R1. *Molecular Microbiology*. **59**: 338-349.

Joshi, B., Schmid, R., Altendorf, K. And Apte, S.K. (2004) Protein recycling is a major component of post-irradiation recovery in *Deinococcus radiodurans* strain R1. *Biochemical and Biophysical Research Communications*. **320**: 1112-1117.

Kamble, V.A., Rajpurohit, Y.S., Srivastava, A.K., and Misra, H.S. (2010) Increased synthesis of signaling molecules coincides with reversible inhibition of nucleolytic activity during postirradiation recovery of *Deinococcus radiodurans*. *FEMS Microbiology Letters*. **303**: 18-25.

Kota, S., and Misra, H.S. (2006) PprA: a protein implicated in radioresistance of *Deinococcus radiodurans* stimulates catalase activity in *Escherichia coli*. *Applied Microbial and Cell Physiology*. **72**: 790-796.

Kota, S., Kumar, C.V., and Misra, H.S. (2010) Characterization of an ATP regulated DNA processing enzyme and thermotolerant phosphoesterase in a

radioresistant bacterium *Deinococcus radiodurans*. *The Biochemical Journal*. **431**: 149-157.

Kowalczykowski, S.C., Dixon, D.A., Eggleston, A.K., Lauder, S.D., and Rehrauer, W.M. (1994) Biochemistry of homologous recombination in *Escherichia coli*. *Microbiological Reviews*. **58**: 401-465.

Krasin, F., and Hutchinson, F. (1977) Repair of DNA double-strand breaks in *Escherichia coli*, which requires *recA* function and the presence of a duplicate genome. *Journal of Molecular Biology*. **116**: 81-98.

Krisko, A., and Radman, M. (2010) Protein damage and death by radiation in *Escherichia coli* and *Deinococcus radiodurans*. *Proceedings of the National Academy of Sciences*. **107**: 14373-14377.

Kuzminov, A. (1995) Collapse and repair of replication forks in *Escherichia coli*. *Molecular Microbiology*. **16**: 373-384.

Lavery, P.E., and Kowalczykowski, S.C. (1992) A postsynaptic role for single-stranded DNA-binding protein in *recA* protein-promoted DNA strand exchange. *Journal of Biological Chemistry*. **267**: 9315-9320.

Levin-Zaidman, S., Englander, J., Shimoni, E., Sharma, A.K., Minton, K.W., and Minsky, A. (2003) Ringlike structure of the *Deinococcus radiodurans* genome: a key to radioresistance?. *Science*. **299**: 254-256.

Liu, Y., Zhou, J., Omelchenko, M.V., Beliaev, A.S., Venkateswaran, A., Stair, J., Wu, L., Thompson, D.K., Xu, D., Rogozin, I.B., Gaidamakova, E.K., Zhai, M., Makarova, K.S., Koonin, E.V., and Daly, M.J. (2003) Transcriptome dynamics of *Deinococcus radiodurans* recovering from ionizing radiation. *Proceedings of the National Academy of Sciences*. **100**: 4191-4196.

Lovett, S.T., and Kolodner, R.D. (1989) Identification and purification of a single-stranded-DNA-specific exonuclease encoded by the *recJ* gene of *Escherichia coli*. *Proceedings of the National Academy of Sciences*. **86**: 2627-2631.

Lu, H., Gao, G., Xu, G., Fan, L., Yin, L., Shen, B., and Hua, Y. (2009) *Deinococcus radiodurans* PprI switches on DNA damage response and cellular

survival networks after radiation damage. *Molecular and Cellular Proteomics*. **8**: 481-494.

Makarova, K.S., Aravind, L., Wolf, Y.I., Tatusov, R.L., Minton, K.W., Koonin, E.V., and Daly, M.J. (2001) Genome of the extremely radiation-resistant bacterium *Deinococcus radiodurans* viewed from the perspective of comparative genomics. *Microbiology and Molecular Biology Reviews*. **65**: 44-79.

Makarova, K.S., Omelchenko, M.V., Gaidamakova, E.K., Matrosova, V.Y., Vasilenko, A., Zhai, M., Lapidus, A., Copeland, A., Kim, E.L., Land, M. *et al.*(2007) *Deinococcus geothermalis*: The pool of extreme radiation resistance genes shrinks. *PLoS ONE*. **2**: 955-

Makharashvili, N., Koroleva, O., Bera, S., Grandgenett, D.P., and Korolev, S. (2004) A novel structure of DNA repair protein RecO from *Deinococcus radiodurans*. *Structure*. **10**: 1881-1889.

Markillie, L.M., Varnum, S.M., Hradecky, P., and Wong, K.K. (1999) Targeted mutagenesis by duplication insertion in the radioresistant bacterium *Deinococcus radiodurans*: radiation sensitivities of catalase (*katA*) and superoxide dismutase (*sodA*) mutants. *Journal of Bacteriology*. **181**: 666-669.

Mijakovic, I., Petranovic, D., Macek, B., Cepo, T., Mann, M., Davies, J., Jensen, P.R., and Vujaklija, D. (2006) Bacterial single-stranded DNA-binding proteins are phosphorylated on tyrosine. *Nucleic Acids Research*. **34**: 1588-1596.

Minton, K.W. (1994) DNA repair in the extremely radioresistant bacterium *Deinococcus radiodurans*. *Molecular Microbiology*. **13**. 9-15.

Modesti, M., Hesse, J.H., and Gellert, M. (1999) DNA binding of XRCC4 protein is associated with V(D)J recombination but not with stimulation of DNA Ligase IV activity. *The EMBO Journal* **7**: 2008-2018.

Morimatsu, K., and Kowalczykowski, S.C. (2003) RecFOR proteins load RecA protein onto gapped DNA to accelerate DNA strand exchange: a universal step of recombinational repair. *Molecular Cell*. **11**: 1337-1347.

Moseley, B.E., and Mattingly, A. (1971) Repair of irradiation transforming deoxyribonucleic acid in wild type and a radiation-sensitive mutant of *Micrococcus radiodurans*. *Journal of Bacteriology*. **105**: 976-983.

Murakami, M., Narumi, S., Satoh, K., Furukawa, A. And Hayata, I. (2006) Analysis of interaction between DNA and *Deinococcus radiodurans* PprA protein by atomic force microscopy*. Biochimica et Biophysica Acta*. **1764**: 20-23.

Narumi, I., Cherdchu, K., Kitayama, S., and Watanabe, H. (1997) The *Deinococcus radiodurans uvrA* gene: identification of mutation sites of two mitomycin-sensitive strains and the first discovery of insertion sequence element from deinobacteria. *Gene*. **198**: 115-126.

Narumi, I., Satoh, K., Cui, S., Funayama, T., Kitayama, S., and Watanabe, H. (2004) PprA: a novel protein from *Deinococcus radiodurans* that stimulates DNA ligation. *Molecular Microbiology*. **54**: 278-285.

Norais, C.A., Chitteni-Pattu, S., Wood, E.A., Inman, R.B., and Cox, M.M. (2009) DdrB protein, an alternative *Deinococcus radiodurans* SSB induced by ionizing radiation. *The Journal of Biological Chemistry*. **284**: 21402-21411.

Pardo, B., Gomez-Gonzalez, B., and Aguilera, A. (2009) DNA repair in mammalian cells: DNA double-strand break repair: How to fix a broken relationship. *Cellular and Molecular Life Sciences*. **66**: 10309-1056.

Pukall, R., Zeytun, A., Lucas, S., Lapidus, A., Hammon, N., Deshpande, S., Nolan, M., Cheng, J.F., Pitluck, S., Liolios, K., Pagani, I., Mikhailova, N., Ivanova, N., Mavromatis, K., Pati, A., Tapia, R., Han, C., Goodwin, L., Chen, A., Palaniappan, K., Land, M., Hauser, L., Chang, Y.J., Jeffries, C.D., Brambilla, E.M., Rohde, M., Göker, M., Detter, J.C., Woyke, T., Bristow, J., Eisen, J.A., Markowitz, V., Hugenholtz, P., Kyrpides, N.C., and Klenk, H.P. (2011) Complete genome sequence of *Deinococcus maricopensis* type strain (LB-34). *Standards in Genomic Sciences*. **4**: 163-172.

Rajpurohit, Y.S., Gopalakrishnan, R., and Misra, H.S. (2008) Involvement of a protein kinase activity inducer in DNA double strand break repair and radioresistance of *Deinococcus radiodurans*. *Journal of Bacteriology*. **190**: 3948-3954.

Rajpurohit, Y.S., and Misra, H.S. (2010) Characterization of a DNA damage-inducible membrane protein kinase from *Deinococcus radiodurans* and its role in bacterial radioresistance and DNA strand break repair. *Molecular Microbiology*. **77**: 1470-1482.

Repine, J.E., Pfenninger, O.W., Talmage, D.W., Berger, E.M., and Pettijohn, D.E. (1981) Dimethyl sulfoxide prevents DNA nicking mediated by ionizing radiation or iron/hydrogen peroxide-generated hydroxyl radical. *Proceedings of the National Academy of Sciences*. **78**: 1001-1003.

Sancar, A., Lindsey-Boltz, L.A., Unsal-Kaçmaz, K., and Linn, S. (2004) Molecular mechanisms of mammalian DNA repair and the DNA damage checkpoints. *Annual Review of Biochemistry*. **73**: 39-85.

Seib, K.L., Tseng, H.J., McEwan, A.G., Apicella, M.A., and Jennings, M.P. (2004) Defenses against oxidative stress in *Neisseria gonorrhoeae* and *Neisseria meningitides*: distinctive systems for different lifestyles. *The Journal of Infectious Diseases*. **190**: 136-147.

Servant, P., Jolivet, E., Bentchikou, E., Mennecier, S., Bailone, A. And Sommer, S. (2007) The ClpPX protease is required for radioresistance and regulates cell division after gamma-irradiation in *Deinococcus radiodurans*. *Molecular Microbiology*. **66**: 1231-1239.

Slade, D., Lindner, A.B., Paul, G., and Radman, M. (2009) Recombination and replication in DNA repair of heavily irradiated *Deinococcus radiodurans*. *Cell*. **136**: 1044-1055.

Slade, D., and Radman, M. (2011) Oxidative stress resistance in *Deinococcus radiodurans*. *Microbiology and Molecular Biology Reviews*. **75**: 133-191.

Solinger, J.A., Kiianitsa, K., and Heyer, W.D. (2002) Rad54, a Swi2/Snf2-like recombinatorial repair protein, disassembles Rad51:dsDNA filaments. *Molecular Cell*. **10**: 1175-1188.

Spagnolo, L., Rivera-Calzada, A., Pearl, L.H. and Llorca, O. (2006) Three dimensional structure of the human DNA-PKcs/Ku70/Ku80 complex assembled on DNA and its implications for DNA DSB repair. *Molecular Cell* **22**: 511-519.

Stracker, T.H., and Petrini, J.H. (2011) The MRE11 complex: starting from the ends. *Nature Reviews Molecular Cell Biology*. **12**: 90-103.

Sugiman-Marangos, S. and Junop, M.S. (2010) The structure of DdrB from *Deinococcus*: a new fold for single-stranded DNA binding proteins. *Nucleic Acids Research*. **38**: 3432-3440.

Symington, L.S., and Gautier, J. (2011) Double-strand break end resection and repair pathway choice. *Annual Review of Genetics*. **45**: 247-271.

Tanaka, M., Eisen, M.A., Peterson, S.N., and Battista, J.R. (2004) Analysis of *Deinococcus radiodurans*` transcriptional response to ionizing radiation and desiccation reveals novel proteins that contribute to extreme radioresistance. *Genetics*. **168**: 21-33.

Tian, B., Wu, Y., Sheng, D., Zheng, Z., Gao, G., and Hua, Y. (2004) Chemiluminescence assay for reactive oxygen species scavenging activities and inhibition of oxidative damage of DNA in *Deinococcus radiodurans*. *Luminescence*. **19**: 78-84.

Timmins, J., Leiros, I., and McSweeney, S. (2007) Crystal structure and mutational study of RecOR provide insight into its mode of DNA binding. *The EMBO Journal*. **26**: 3260-3271.

Venkateswaran, A., McFarlan, S.C., Ghostal, D., Minton, K.W., Vasilenko, E., Makarova, K., Wackett, L.P., and Daly, M.J. (2000) Physiologic determinants of radiation resistance in *Deinococcus radiodurans*. *Applied Environmental Microbiology*. **66**: 2620-2626.

Vukovic-Nagy, B., Fox, B.W., and Fox, M. (1974) The release of a deoxyribonucleic acid fragment after x-irradiation of *Micrococcus radiodurans*. *International Journal of Radiation Biology and Related Studies in Physics, Chemistry, and Medicine*. **25**: 329-337.

Walker, J.R., Corpina, R.A., and Goldberg, J. (2001) Structure of Ku heterodimer bound to DNA and its implications for double-strand break repair. *Nature*. **412**: 607-614.

White, O., Eisen, J.A., Heidelberg, J.F., Hickey, E.K., Peterson, J.D., Dodson, R.J., Haft, D.H., Gwinn, M.L., Nelson, W.C., Richardson, D.L., Moffat, K.S., Qin, H., Jiang, L., Pamphile, W., Crosby, M., Shen, M., Vamathevan, J.J., Lam, P., McDonald, L., Utterback, T., Zalewski, C., Makarova, K.S., Aravind, L., Daly, M.J., Minton, K.W., Fleischmann, R.D., Ketchum, K.A., Nelson, K.E., Salzberg, S., Smith, H.O., Venter, J.C., and Fraser, C.M. (1999) Genome sequence of the radioresistant bacterium *Deinococcus radiodurans* R1. *Science*. **286**: 1571-1577.

Xu, G., Wang, L., Chen, H., Lu, H., Ying, N., Tian, B., and Hua, Y. (2008) RecO is essential for DNA damage repair in *Deinococcus radiodurans*. *Journal of Bacteriology*. **190**: 2624-2628.

Xu, G., Lu, H., Wang, L., Chen, H., Xu, Z., Hu, Y., Tian, B., and Hua, Y. (2010) DdrB stimulates single-stranded DNA annealing and facilitates RecA-independent DNA repair in *Deinococcus radiodurans*. *DNA Repair (Amst.)*. **9**: 805-812.

Yuan, M., Chen, M., Zhang, W., Lu, W., Wang, J., Yang, M., Zhao, P., Tang, R., Li, X., Hao, Y., Zhou, Z., Zhan, Y., Yu, H., Teng, C., Yan, Y., Ping, S., Wang, Y., and Lin, M. (2012) Genome sequence and transcriptome analysis of the radioresistant bacterium *Deinococcus gobiensis*: insights into the extreme environmental adaptations. *PLoS ONE*. **7**: e34458

Zahradka, K., Slade, D., Bailone, A., Sommer, S., Averbeck, D., Petranovic, M., Lindner, A.B., and Radman, M. (2006) Reassembly of shattered chromosomes in *Deinococcus radiodurans*. *Nature*. **443**: 569-573.

Zimmerman, J.M., and Battista, J.R. (2005) A ring-like nucleoid is not necessary for radioresistance in the *Deinococcaceae*. *BMC Microbiology*. **5**: 17.

APPENDIX A.

Table 3. Crystallization conditions that resulted in crystals of PprA

PprA from *D. geothermalis*

Crystallization Kit - Condition #	Initial Condition Components	Additive Condition Components
Nextal Classics - #7	0.1M tri-sodium citrate pH 5.6, 20% (v/v) isopropanol, 20% (w/v) PEG 4000	N/A
Nextal Classics - #25	0.4M ammonium phosphate	N/A
MCSG II - #33	0.2 M Sodium Fluoride, 20% (w/v) PEG 3350	N/A
MCSG II - #35	0.1 M Bis-Tris Propane:HCl pH 7.0 1.3 M Ammonium Tartrate Dibasic	N/A
MCSG II - #47	0.1 M Tris:HCl pH 8.5, 1.5 M Lithium Sulfate	N/A
MCSG II - #61	0.2 M Sodium Chloride, 0.1 M Imidazole:HCl pH 8.0, 1.0 M Ammonium Phosphate Dibasic	N/A
MCSG III - #4	0.1 M Imidazole:HCl pH 8.0, 1.0 M Ammonium Phosphate Dibasic	N/A
MCSG III - #31	0.1 M Bis-Tris Propane:HCl pH 7.0 1.0 M Ammonium Citrate Tribasic pH 7.0	N/A
MCSG IV - #44	0.2 M Lithium Sulfate, 0.1 M Sodium Citrate:Citric Acid pH 5.5, 15% (v/v) Ethanol	N/A
MCSG III - #4 + HAS - #52	0.1 M Imidazole:HCl pH 8.0, 1.0 M Ammonium Phosphate Dibasic	40% v/v Pentaerythritol ethoxylate (3/4 EO/ON)
Homemade Condition + HDS #3	0.1 M Ammonium phosphate monobasic, 2% glycerol	0.46 mM Dodecyltrimethylammonium chloride

$PprA_{9\text{-}284}$ from *D. radiodurans*

Crystallization Kit - Condition #	Initial Condition Components	Additive Condition Components
Nextal Classics - #9	0.2 M tri-Sodium citrate, 0.1 M Sodium cacodylate pH 6.5, 30 %(v/v) Isopropanol	N/A
Nextal Classics - #12	1.5 M Sodium chloride, 10 %(v/v) Ethanol	N/A
Nextal Classics - #22	0.1 M HEPES pH 7.5, 70 %(v/v) MPD	N/A
Nextal Classics - #38	0.1 M Imidazole pH 6.5, 1.0 M Sodium acetate	N/A
MCSG I - #20	0.17 M Sodium Acetate, 0.085 M Tris:HCl pH 8.5, 25.5% (w/v) PEG 4000, 15% (v/v) Glycerol	N/A

MCSG I - #29	0.2 M Magnesium Acetate, 20% (w/v) PEG 3350	N/A
MCSG I - #45	0.2 M Sodium Chloride, 0.1 M Tris:HCl pH 8.5, 25% (w/v) PEG 3350	N/A
MCSG I - #86	0.2 M Potassium Iodide, 20% (w/v) PEG 3350	N/A
MCSG I - #92	1.0 M Succinic Acid pH 7.0, 0.1 M HEPES:NaOH pH 7.0, 1% (w/v) PEG MME 2000	N/A
MCSG II - #2	0.15 M Potassium Bromide, 30% (w/v) PEG MME 2000	N/A
MCSG II - #18	0.2 M Sodium Formate, 20% (w/v) PEG 3350	N/A
MCSG II - #22	1.1 M Sodium Malonate pH 7.0, 0.1 M HEPES:NaOH pH 7.0, 0.5% (v/v) Jeffamine® ED-2001 pH 7.0	N/A
MCSG II - #26	0.64 M Malonic Acid, 0.088 M Ammonium Citrate Tribasic, 0.042 M Succinic Acid, 0.105 M 26 C2 DL-Malic Acid, 0.14 M Sodium Acetate, 0.175 M Sodium Formate, 0.056 M Ammonium Tartrate Dibasic, Final pH 7.0	N/A
MCSG II - #30	0.1 M BICINE:NaOH pH 9 20% (w/v) PEG 6000	N/A
MCSG II - #49	0.1M Bis-Tris Propane:HCl pH 7.0 1.8 M Sodium Acetate pH 7.0	N/A
MCSG II - #65	0.02 M Magnesium Chloride 0.1 M HEPES:NaOH pH 7.5 22% (w/v) Polyacrylic Acid 5100	N/A
MCSG III - #46	0.2 M Potassium Citrate Tribasic pH 8.3, 20% (w/v) PEG 3350	N/A
Nextal Classics #9 + HAS #22	0.2 M tri-Sodium citrate, 0.1 M Sodium cacodylate pH 6.5, 30 %(v/v) Isopropanol	1.0 M Potassium sodium tartrate tetrahydrate
Nextal Classics #9 + HAS #25	0.2 M tri-Sodium citrate, 0.1 M Sodium cacodylate pH 6.5, 30 %(v/v) Isopropanol	1.0 M Sodium malonate pH 7.0
Nextal Classics #9 + HAS #38	0.2 M tri-Sodium citrate, 0.1 M Sodium cacodylate pH 6.5, 30 %(v/v) Isopropanol	0.1 M Spermidine
Nextal Classics #9 + HAS #51	0.2 M tri-Sodium citrate, 0.1 M Sodium cacodylate pH 6.5, 30 %(v/v) Isopropanol	30% w/v Dextran sulfate sodium salt
Nextal Classics #9 + HAS #68	0.2 M tri-Sodium citrate, 0.1 M Sodium cacodylate pH 6.5, 30 %(v/v) Isopropanol	0.15 mM CYMAL®-7
MCSG II #26 + Opti Salts #79	0.64 M Malonic Acid, 0.088 M Ammonium Citrate Tribasic, 0.042 M Succinic Acid, 0.105 M 26 C2 DL-Malic Acid, 0.14 M Sodium Acetate, 0.175 M Sodium Formate, 0.056 M Ammonium Tartrate	0.1 M Sodium acetate pH 4.6, 3.5 M Sodium nitrate

	Dibasic, Final pH 7.0	
MCSG II #26 + Opti Salts #80	0.64 M Malonic Acid, 0.088 M Ammonium Citrate Tribasic, 0.042 M Succinic Acid, 0.105 M 26 C2 DL-Malic Acid, 0.14 M Sodium Acetate, 0.175 M Sodium Formate, 0.056 M Ammonium Tartrate Dibasic, Final pH 7.0	3.5 M Sodium nitrate
MCSG II #26 + Opti Salts #91	0.64 M Malonic Acid, 0.088 M Ammonium Citrate Tribasic, 0.042 M Succinic Acid, 0.105 M 26 C2 DL-Malic Acid, 0.14 M Sodium Acetate, 0.175 M Sodium Formate, 0.056 M Ammonium Tartrate Dibasic, Final pH 7.0	0.1 M Sodium acetate pH 4.6, 1.75 M Sodium nitrate
MCSG II #26 + Opti Salts #92	0.64 M Malonic Acid, 0.088 M Ammonium Citrate Tribasic, 0.042 M Succinic Acid, 0.105 M 26 C2 DL-Malic Acid, 0.14 M Sodium Acetate, 0.175 M Sodium Formate, 0.056 M Ammonium Tartrate Dibasic, Final pH 7.0	1.75 M Sodium nitrate
MCSG II #26 + HDS #58	0.64 M Malonic Acid, 0.088 M Ammonium Citrate Tribasic, 0.042 M Succinic Acid, 0.105 M 26 C2 DL-Malic Acid, 0.14 M Sodium Acetate, 0.175 M Sodium Formate, 0.056 M Ammonium Tartrate Dibasic, Final pH 7.0	250 mM MEGA-9
MCSG III - #46 + HDS #14	0.2 M Potassium Citrate Tribasic pH 8.3, 20% (w/v) PEG 3350	10% w/v ANAPOE®-20
MCSG III - #46 + HDS #36	0.2 M Potassium Citrate Tribasic pH 8.3, 20% (w/v) PEG 3350	18 mM n-Decyl-b-D-maltoside
MCSG III - #46 + HDS #73	0.2 M Potassium Citrate Tribasic pH 8.3, 20% (w/v) PEG 3350	0.5 M NDSB-195
MCSG III - #46 + HDS #78	0.2 M Potassium Citrate Tribasic pH 8.3, 20% (w/v) PEG 3350	4.0 mM ZWITTERGENT® 3-14
MCSG III - #46 + OS #51	0.2 M Potassium Citrate Tribasic pH 8.3, 20% (w/v) PEG 3350	0.1 M Tris-HCl pH 8.5, 3.5 M Sodium formate
MCSG III - #46 + OS #94	0.2 M Potassium Citrate Tribasic pH 8.3, 20% (w/v) PEG 3350	0.1 M Sodium acetate pH 4.6, 2 M Lithium chloride
MCSG III - #46 + HAS #28	0.2 M Potassium Citrate Tribasic pH 8.3, 20% (w/v) PEG 3350	30% v/v Dimethyl sulfoxide
MCSG III - #46 + HAS #48	0.2 M Potassium Citrate Tribasic pH 8.3, 20% (w/v) PEG 3350	0.01 M GSH (L-Glutathione reduced), GSSG (L-Glutathione oxidized)
MCSG III - #46 + HAS #73	0.2 M Potassium Citrate Tribasic pH 8.3, 20% (w/v) PEG 3350	30% w/v Trimethylamine N-oxide dihydrate
MCSG III - #46 + HAS #96	0.2 M Potassium Citrate Tribasic pH 8.3 20% (w/v) PEG 3350	40% v/v 1,1,1,3,3,3-Hexafluoro-2-propanol
MCSG III - #46 + SB #1	0.2 M Potassium Citrate Tribasic pH 8.3 20% (w/v) PEG 3350	0.33% w/v 1,5-Naphthalenedisulfonic acid disodium salt

		0.33% w/v 2,5-Pyridinedicarboxylic acid, 0.33% w/v 3,5-Dinitrosalicylic acid, 0.02 M HEPES sodium pH 6.8
MCSG III - #46 + SB #4	0.2 M Potassium Citrate Tribasic pH 8.3, 20% (w/v) PEG 3350	0.25% w/v 3,5-Dinitrosalicylic acid, 0.25% w/v 4-Aminobenzoic acid, 0.25% w/v Salicylic acid, 0.25% w/v Trimesic acid, 0.02 M HEPES sodium pH 6.8
MCSG III - #46 + SB #69	0.2 M Potassium Citrate Tribasic pH 8.3, 20% (w/v) PEG 3350	0.2% w/v 6-Aminohexanoic acid, 0.2% w/v Benzamidine hydrochloride, 0.2% w/v Congo Red, 0.2% w/v Nicotinamide, 0.2% w/v Salicin, 0.02 M HEPES sodium pH 6.8
MCSG III - #46 + SB #72	0.2 M Potassium Citrate Tribasic pH 8.3, 20% (w/v) PEG 3350	0.11% w/v Dodecanedioic acid, 0.11% w/v Fumaric acid, 0.11% w/v Glutaric acid, 0.11% w/v Hexadecanedioic acid, 0.11% w/v Maleic acid, 0.11% w/v Oxamic acid, 0.11% w/v Pimelic acid, 0.11% w/v Sebacic acid, 0.11% w/v Suberic acid, 0.02 M HEPES sodium pH 6.8

APPENDIX B

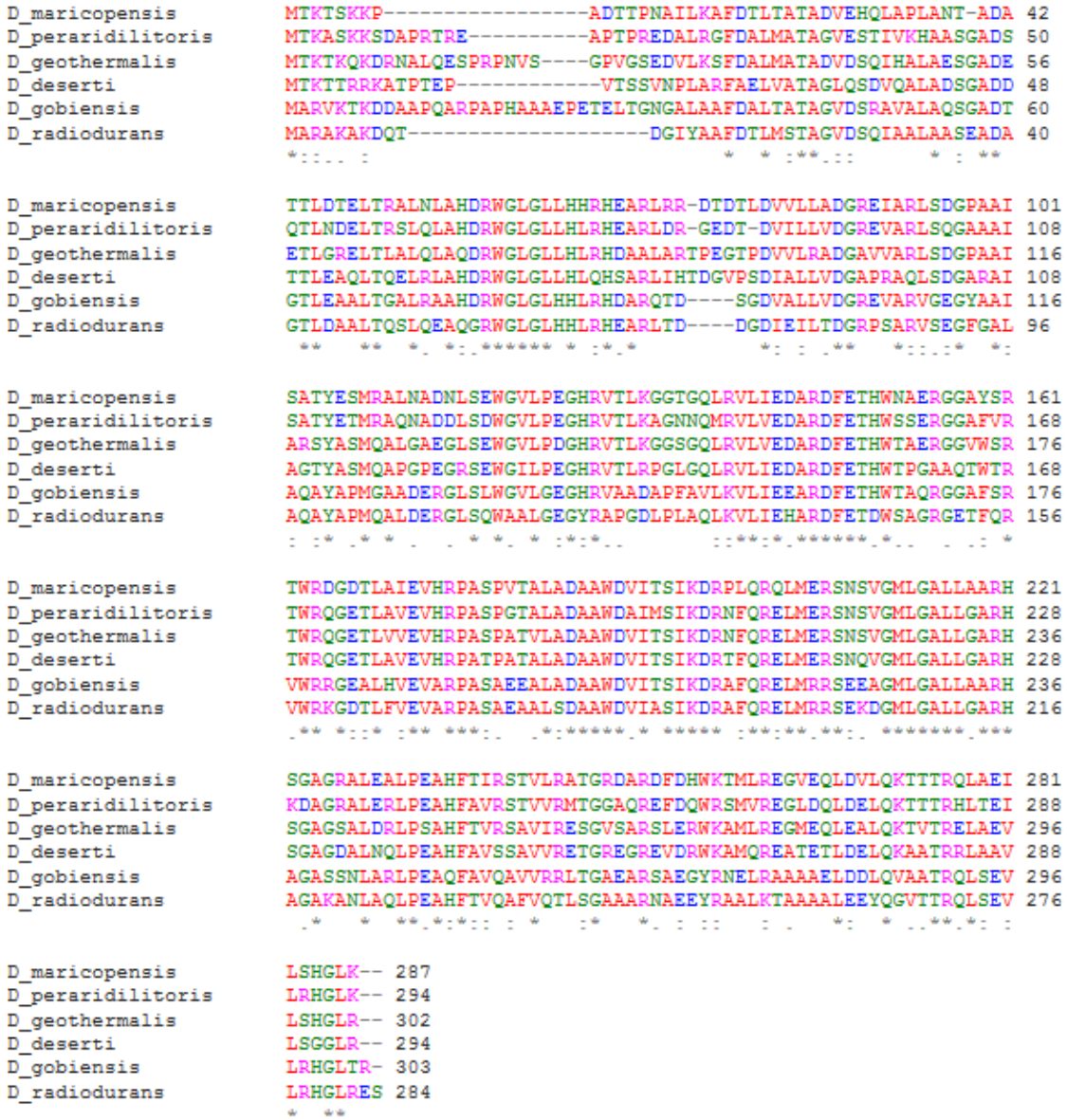

Figure B. – Multiple sequence alignment of PprA from various *Deinococcus* spp. Colours identify residues according to their physiochemical properties. Red: small + hydrophobic (including aromatic - Y); Blue: acidic; Magenta: basic - H; Green: hydroxyl + sulfhydryl + amine + G. Asterisk (*) indicates positions which have a single, fully conserved residue. Colon (:) indicates conservation between groups of strongly similar properties. Period (.) indicates conservation between groups of weakly similar properties.

APPENDIX C

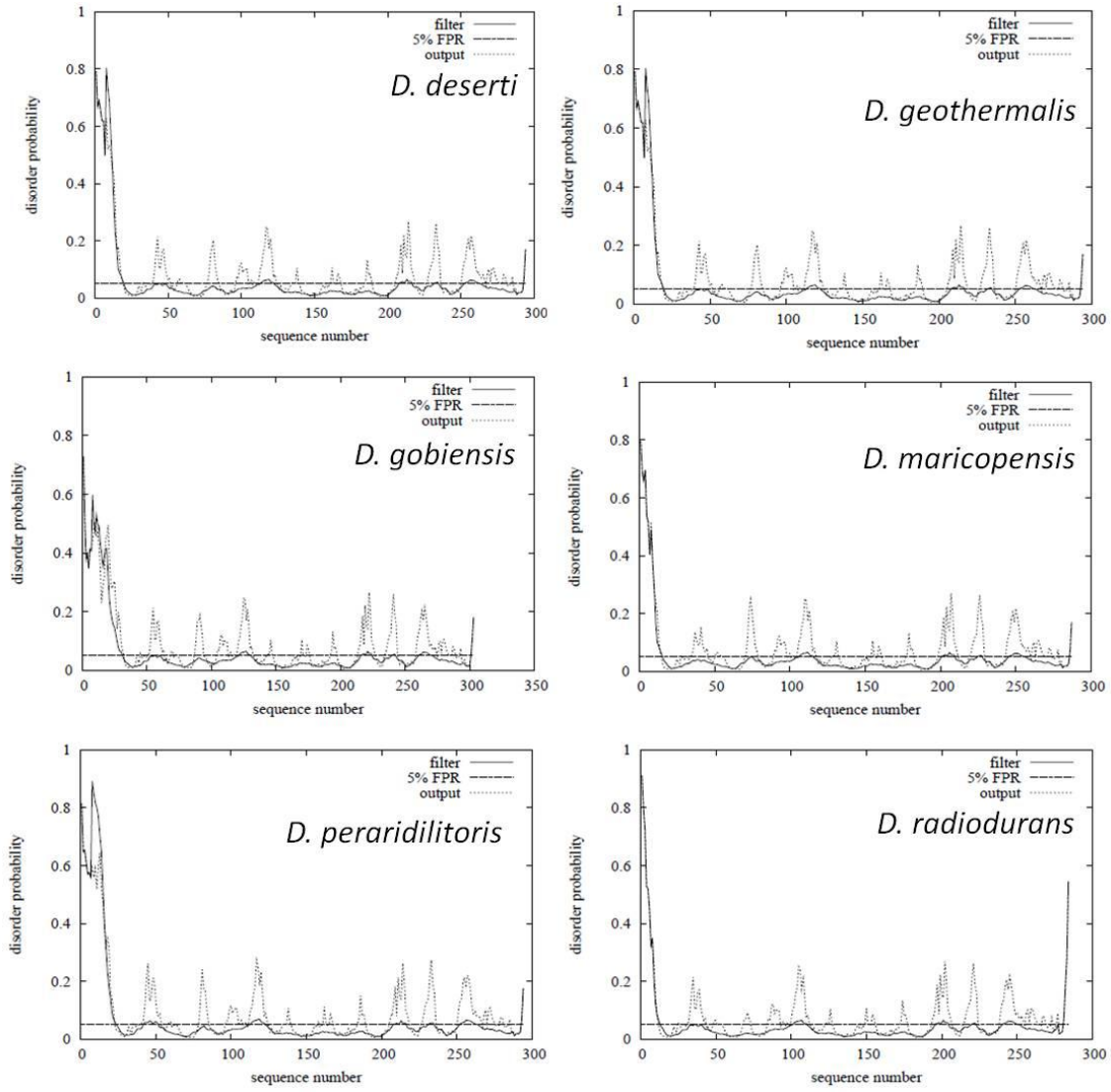

Figure C. – The disorder profiles of PprA from various *Deinococcus* spp. generated using PSIPRED DISOPRED2 prediction tool. The y-axis displays the probability of disorder, while the x-axis displays the amino acid sequence of the protein. The data predicts that the N-terminus of each PprA protein (the first ~25 amino acid residues) is very highly disordered.

APPENDIX D.

PprA from *D. deserti* PprA from *D. geothermalis*

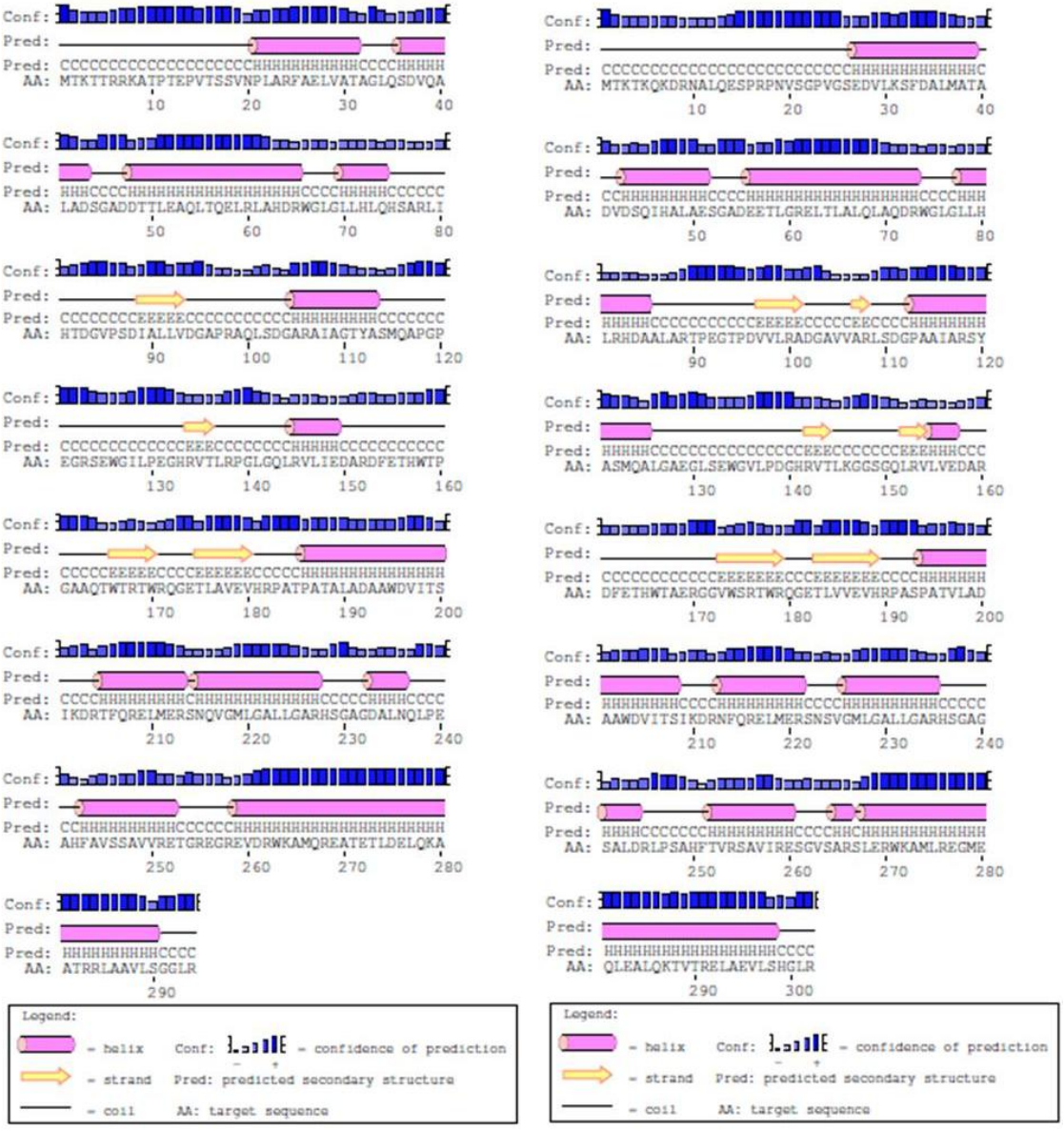

Figure D. – Secondary structure prediction models of PprA from six *Deinococcus* spp. generated using PSIPRED. Secondary structure is displayed as an α-helix (pink rod), β-sheet (yellow arrow) or a random coil (black line). Species are displayed in alphabetical order.

APPENDIX D. CONTINUED

PprA from *D. gobiensis* PprA from *D. maricopensis*

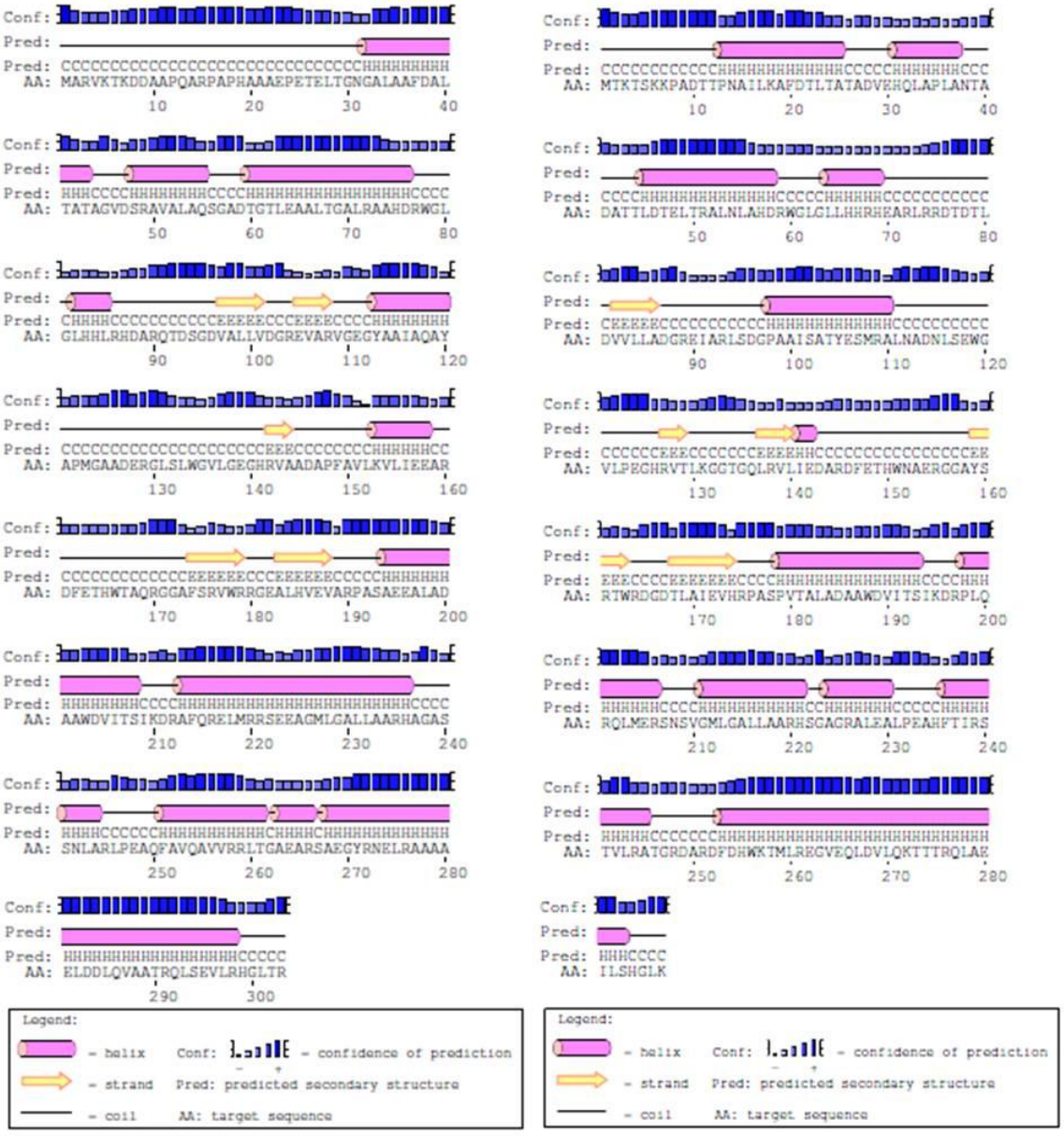

Figure D. – Secondary structure prediction models of PprA from six *Deinococcus* spp. generated using PSIPRED. Secondary structure is displayed as an α-helix (pink rod), β-sheet (yellow arrow) or a random coil (black line). Species are displayed in alphabetical order.

APPENDIX D. CONTINUED

PprA from *D. peraridilitoris* PprA from *D. radiodurans*

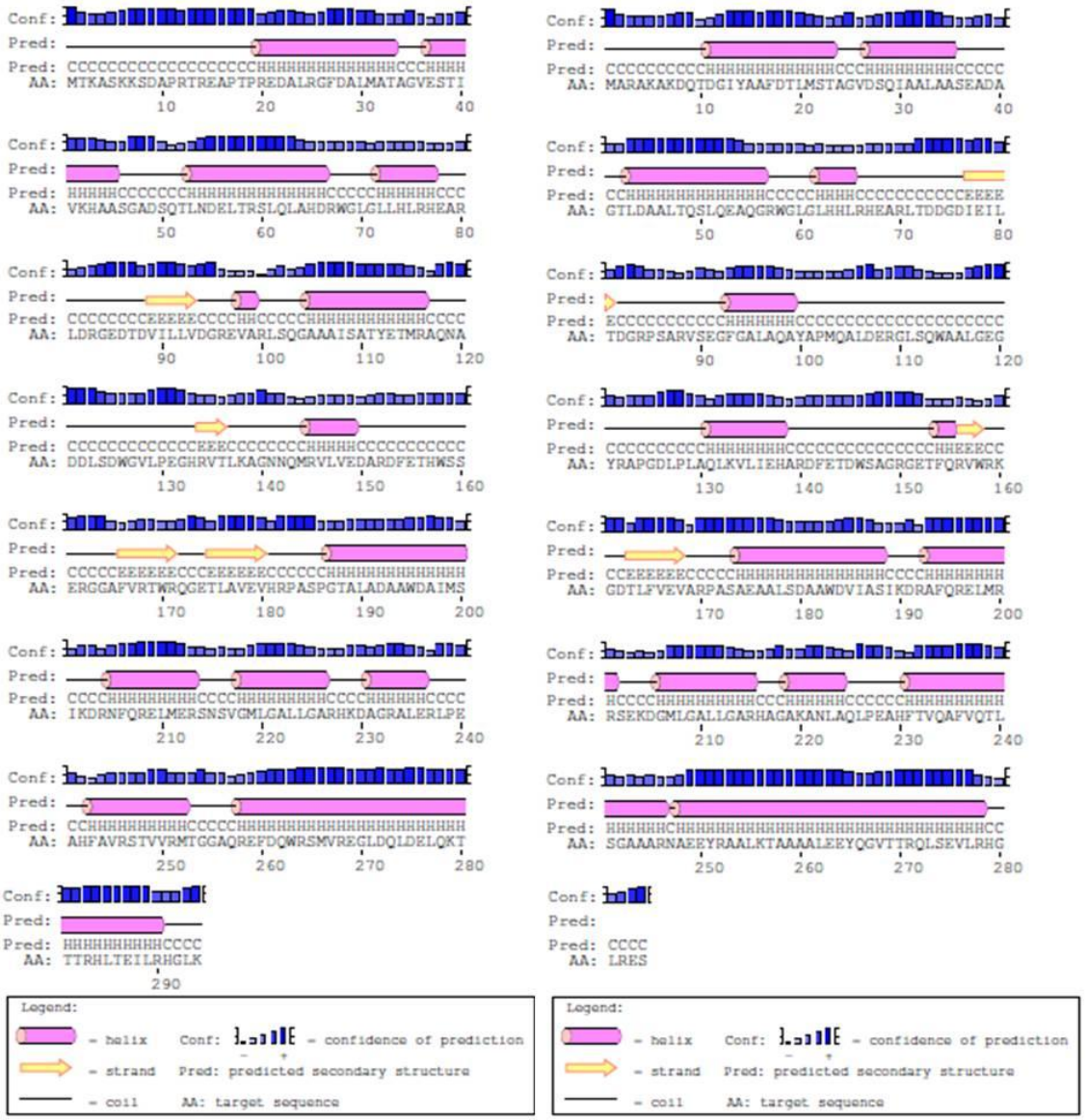

Figure D. – Secondary structure prediction models of PprA from six *Deinococcus* spp. generated using PSIPRED. Secondary structure is displayed as an α-helix (pink rod), β-sheet (yellow arrow) or a random coil (black line). Species are displayed in alphabetical order.